Nano Research
2022, 15(8): 7267–7285

ISSN 1998-0124 CN 11-5974/O4
https://doi.org/10.1007/s12274-022-4385-4

Review Article

Emerging prospects of protein/peptide-based nanoassemblies for drug delivery and vaccine development

Taiyu Liu, Lu Li, Cheng Cheng, Bingfang He, and Tianyue Jiang (✉)

School of Pharmaceutical Sciences, Nanjing Tech University, Nanjing 211816, China

Received: 29 January 2022 / **Revised:** 31 March 2022 / **Accepted:** 1 April 2022

ABSTRACT

Proteins have been widely used in the biomedical field because of their well-defined architecture, accurate molecular weight, excellent biocompatibility and biodegradability, and easy-to-functionalization. Inspired by the wisdom of nature, increasing proteins/peptides that possess self-assembling capabilities have been explored and designed to generate nanoassemblies with unique structure and function, including spatially organized conformation, passive and active targeting, stimuli-responsiveness, and high stability. These characteristics make protein/peptide-based nanoassembly an ideal platform for drug delivery and vaccine development. In this review, we focus on recent advances in subsistent protein/peptide-based nanoassemblies, including protein nanocages, virus-like particles, self-assemblable natural proteins, and self-assemblable artificial peptides. The origin and characteristics of various protein/peptide-based assemblies and their applications in drug delivery and vaccine development are summarized. In the end, the prospects and challenges are discussed for the further development of protein/peptide-based nanoassemblies.

KEYWORDS

drug delivery, vaccine, protein/peptide, self-assembly, targeting, controlled release

1 Introduction

Proteins possess the well-defined architecture created by nature and show promising prospects in the field of biomedicine due to their intrinsic features, including a) good biocompatibility and biodegradability [1–3], b) inherent biological activity [4–7], and c) precise modification. The linear modification of a peptide on the protein or even the fusion of two different proteins can be achieved to precisely generate fusion proteins by genetic engineering [8–10]. d) Abundance of modifiable groups [11–13]. Amino acids, the basic unit of proteins contain a mass of multifunctional groups, such as $-NH_2$, –COOH, and –SH, which can be attached with one or more types of drug molecules, metal ions, ligands, and so on.

Owing to their excellent characteristics, a great variety of proteins have been developed as drug carriers in recent two decades. One of the most well-known proteins is human serum albumin (HSA), which can resist the affinity of macrophages and prolong the blood circulation time of the payloads [14–17]. Through high-pressure homogenization technology, HSA has been used to load paclitaxel (PTX) to obtain Abraxane® with a particle size of 130 nm, which entered the clinic for breast cancer and metastatic pancreatic cancer therapy [18]. Besides, proteins including bovine serum albumin [19–22], gelatin [23–26], zein [27–29], gliadin [30, 31], soy, and whey protein [32–34], have been explored and prepared into nanocarriers to load drugs for improved pharmaceutical property and *in vivo* performance. However, the above-mentioned proteins are not capable of forming micro/nano-particles spontaneously, and thus harsh preparation conditions, like denaturation and crosslinking, or certain equipment are commonly required for the construction of micro/nano-carriers. Another feasible strategy is to introduce hydrophobic groups to endow proteins with amphiphilicity to drive assembly, such as long-chain alkanes [35], polyoxypropylene groups [36], hydrocarbon-containing aryl groups [37], esters [38], and other groups [39].

Interestingly, researchers found that some proteins possess complex and highly ordered structures by supramolecular self-assembly of subunits, such as ferritin (Fn) for iron storage [40, 41]. Inspired by the native utility of protein assemblies for cargo loading, transportation, and protection, increasing efforts have been made to explore and develop assemblable proteins/peptides to construct supramolecular assemblies with excellent biological and physicochemical properties for biomedical application, including drug delivery and vaccine development. In this review, we focus on emerging proteins/peptides with self-assembling capabilities, including protein nanocages, virus-like particles, self-assemblable natural proteins, and self-assemblable artificial peptides. The origin and characteristics of various protein/peptide-based assemblies and their applications in drug delivery and vaccine development are summarized (Fig. 1). The prospects and challenges are discussed in the end for the further development of protein/peptide-based nanoassemblies.

2 Classification of protein/peptide-based nanoassemblies

2.1 Protein nanocages

Some proteins with special functions in living organisms are

Address correspondence to tjiang@njtech.edu.cn

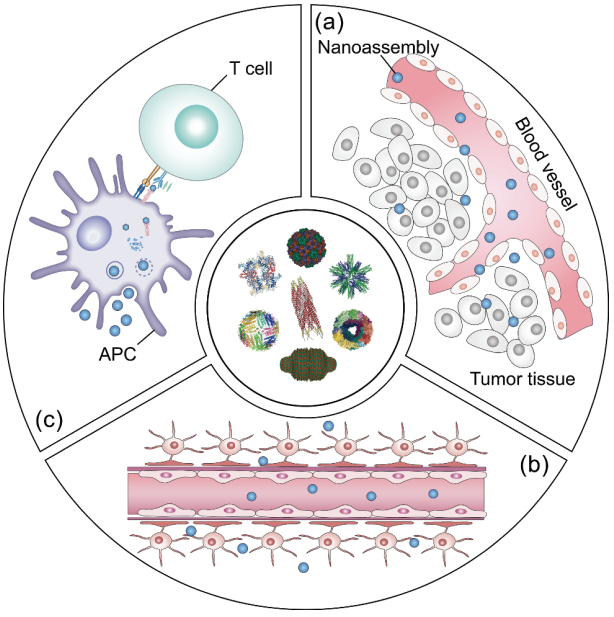

Figure 1 The inner circle represents the structures of different protein/peptide-based nanoassemblies. The outer circle shows the representative applications of protein/peptide-based nanoassemblies for (a) targeted delivery, (b) blood–brain barrier transport, and (c) vaccine therapy.

found to naturally have cage-like structures, which are designated as protein nanocages. These protein nanocages assembled from multiple subunits have an internal cavity structure ranging from tens to hundreds of nanometers, which provide spatial control to biological processes and shield compartmentalized compounds [42]. The quaternary structures of protein cages are typically preserved by multiple weak non-covalent interactions, including hydrophobic interaction, electrostatic interaction, chelation, and other forces. The assembly mechanism of protein nanocages is complex, and there have been many related reports, which are not introduced detailedly in this review [43–46].

2.1.1 *Fn*

Fn, a protein family storing iron, universally exists in almost all kinds of living life including animals, plants, and bacteria [47], and performs essential roles in antioxidation and iron storage [40, 48]. Fn from different species has a similar structure of well-defined cage-like shape assembled from 24 subunits, with an external diameter of 12 nm and an internal diameter of 8 nm (Fig. 2) [49–51]. The subunits are mainly divided into two types, heavy chains (H-chain, 21 kDa) and light chains (L-chain, 19 kDa). The H-chain contains a ferroxidase center that is indispensable for Fe uptake and fast oxidation of Fe(II) ions by oxygen, and the L-chain contains a nucleation site for iron mineralization without the ferroxidase center. The ratio of H-chain to L-chain in the Fn depends on their original organs or tissues and is even affected by pathological conditions [52, 53]. Fn is highly stable at high temperature and possesses pH-induced reversible disassembly and reassembly. These characteristics make Fn a robust carrier and liable to load drugs by pH adjustment [54–59]. Moreover, Fn made of 24 H-chain (HFn) has been confirmed to target various types of tumor cells that overexpress transferrin receptor 1 (TfR1), including lung and breast cancers [60–65]. In addition, since a high level of TfR1 is also detected on the surface of brain capillary endothelial cells, HFn-based nanoassemblies show the capability to transport through the blood–brain barrier (BBB) by receptor-mediated transcytosis [66–68].

2.1.2 *Heat shock protein (HSP)*

HSPs are molecular chaperones that exist in different species from bacteria to humans, whose function is to attach to and stabilize partially or totally unfolded proteins [69–71]. Some members of HSPs (HSP70, HSP40, and HSP60) engage in protein folding under a normal environment, and others (HSP104, inducible HSP70s, and small HSPs (smHSPs)) are proved to play essential roles in organisms prevention from a wide range of biotic and abiotic stress [72, 73]. Composed of 24 subunits, smHSPs are one of the most commonly used HSPs for drug delivery applications and can form octahedral cages ranging in size from 16 to over 40 kDa [74]. Like other protein nanocages, smHSPs consist of the exterior, interior, and interface surfaces with an external and internal diameter of 12 and 6.5 nm, respectively, and a large-size pore of about 3 nm, which allow the exchange of free cargo between the exterior solution and the interior cavity (Fig. 2) [75–77]. smHSPs are relatively stable and robust at the temperature of 70 °C and in the pH range from 4 to 11 [78, 79]. The C-terminal extensions of smHSPs are relatively unstructured and can be applied with various modifications [80]. As smHSPs

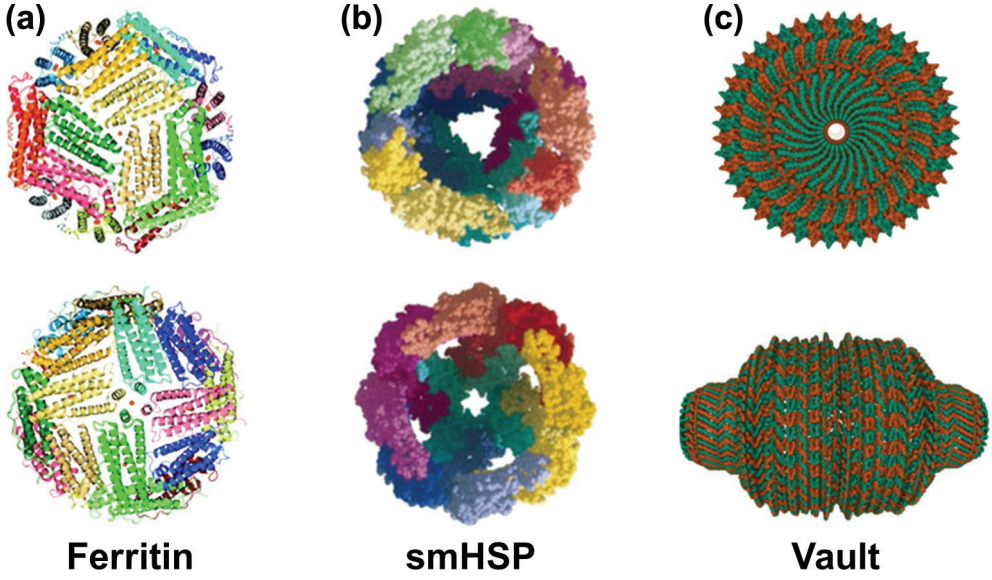

Figure 2 Two different views of the nanocage structures of (a) Bullfrog M ferritin (PDB ID: 4DAS) (reproduced with permission from Ref. [51], © American Chemical Society 2012); (b) smHSP (PDB ID: 1SHS) (reproduced with permission from Ref. [75], © Macmillan Publishers Ltd. 1998); (c) recombinant MVP (*Rattus norvegicus*) of Vault (PDB ID: 6BP7) (reproduced with permission from Ref. [86], © Elsevier Ltd. 2018).

have no cysteine residues in sequence, the mutagenesis of smHSPs can offer spatially site-specific thiol groups on the interior or exterior surfaces for further precise modification [81]. Kawano et al. mutated the glycine at position 41 of smHSP to cysteine (HSPG41C) for the site-specific conjugation with the contrast agent diethylenetriaminepentaacetic acid (DTPA) [82].

2.1.3 *Vault*

Vaults which were first noticed as a contaminant of rat liver coated vesicles in 1986 are the largest known ribonucleoprotein complex in eukaryotic organisms. Vaults were named for their multiple-arched morphology, reminiscent of the ceilings in ancient cathedrals (Fig. 2) [83–86]. It has been concluded that vaults, like the nuclear pore complex, are used to transport large molecules (such as messenger ribonucleic acid (mRNA)) from the nucleus to the cytoplasm, but their definite functions have not been confirmed yet. The vaults in nature consist of major vault protein (MVP, 100 kDa), vault poly(ADP-ribose) polymerase (VPARP, 193 kDa), telomerase associated protein 1 (290 kDa), and several copies of one or more associated RNA. MVP is the main component of the entire nanocage shell [84, 87–89]. The commonly applied recombinant vault-based nanoassemblies only retain MVP subunits which can undergo modification on the interior and exterior surfaces. As the C-terminus of MVP is exposed on the exterior surfaces and the N-terminus is close to the waist, located at the interior of the nanoparticle, it is reasonable to modify the C-terminus with targeting ligands and the N-terminus with therapeutic drugs [90]. In addition, as it was reported that a MVP interaction domain (INT, 17 kDa) derived from the C-terminal of VPARP could interact with MVP after incubating on ice, fusing INT into protein drug is a flexible and convenient strategy to construct various agent-vault nanoassemblies [91]. Vaults can keep stable at pH from 4 to 8 and temperatures from 10 to 90 °C, but irreversibly disassemble into halves at pH from 3 to 4 [92, 93].

2.2 Virus-like particle (VLP)

VLPs are nanostructures assembled from viral structural proteins. Due to the lack of viral genome, VLPs are replication-deficient and every kind of VLPs owns its unique structure (Fig. 3) [94–98]. The VLP from hepatitis B virus is composed of 240 coat proteins, and the VLP from P22 bacteriophage, one of the largest known icosahedral VLPs, is composed of approximately 420 coat proteins. These different kinds of VLPs show multitudinous sizes, ranging from 18 to 500 nm. Besides, VLPs from plant viruses including CPMV, CCMV, and PhMV, and bacteriophages including P22, Qβ and MS2 are non-infectious in mammals [99, 100], which have been demonstrated to be an effective platform for delivering multiple therapeutic molecules such as small molecular drugs, short peptides, proteins, and nucleic acids [101–103]. More than serving as a drug delivery carrier, VLPs are also suitable for utilization as vaccine platforms because they can display antigenic epitopes in a multimeric, repetitive, and highly spatially organized conformation, which is conducive to stimulating both humoral and cellular immune responses [104–108].

2.3 Self-assemblable natural proteins

Distinguished from protein nanocages, which have special cage-like structures through the regular arrangement of protein subunits, self-assemblable natural proteins can form nanometric multimers through the self-assembly of multiple copies of one protein.

2.3.1 *Hydrophobin (HFB)*

HFBs are a sort of small, secreted proteins ubiquitous in the aerial hyphae of fungi and fruiting body surfaces [109, 110]. The extraordinary surface activity of HFBs comes from their unique amphipathic structures, which contain hydrophilic end and hydrophobic patch on the surface [109]. HFBs generally consist of less than 100 amino acids with 8 highly conserved cysteine residues. The correct formation of four disulfide bonds is indispensable to stabilizing the spatial structure of HFBs. It has been found that secreted HFBs are soluble in aqueous at low concentrations and form multimers to reach an energetically favorable state at high concentrations. When in contact with a hydrophilic/hydrophobic interface, HFBs can arrange into an amphipathic membrane [111].

HFBs are mainly discriminated into two classes, class I and class II based on their structure formed by self-assembly at the oil–water interface, hydropathic plots, and solubility characteristics [110, 112, 113]. Generally, class II HFB has higher water solubility than class I HFB. SC3 from *Schizophyllum commune*, as the most extensively investigated class I HFB, can form amyloid-like rodlets at hydrophilic and hydrophobic interfaces. HFBI or HFBII from *Trichoderma reesei* as representatives of class II HFB, self-assembles into a highly ordered two-dimensional (2D) crystalline monolayer at two-phase interfaces (Fig. 4) [114]. Both two classes of HFBs could self-assemble into nanoparticles for dissolution and sustained release of encapsulated water-insoluble drugs [115, 116].

2.3.2 *Casein*

Caseins, a family of secreted calcium phosphate-binding phosphoproteins [117], are the main ingredient of mammalian milk, accounting for 80% of total bovine milk proteins [118]. Caseins are a mixture of four phosphoproteins, α_{S1}-, α_{S2}-, β-, and

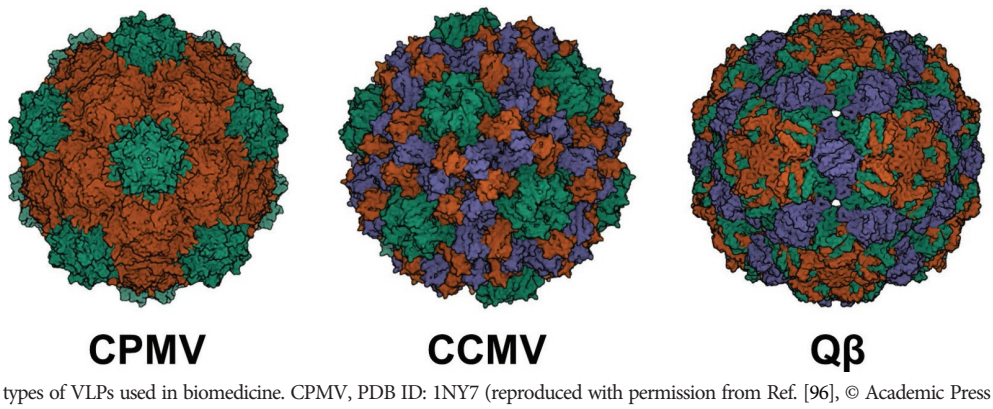

Figure 3 Different types of VLPs used in biomedicine. CPMV, PDB ID: 1NY7 (reproduced with permission from Ref. [96], © Academic Press 1999); CCMV, PDB ID: 1ZA7 (reproduced with permission from Ref. [97], © American Society for Microbiology 2006); Qβ, PDB ID: 5VLY (reproduced with permission from Ref. [98], © Cui, Z. C. et al. 2017).

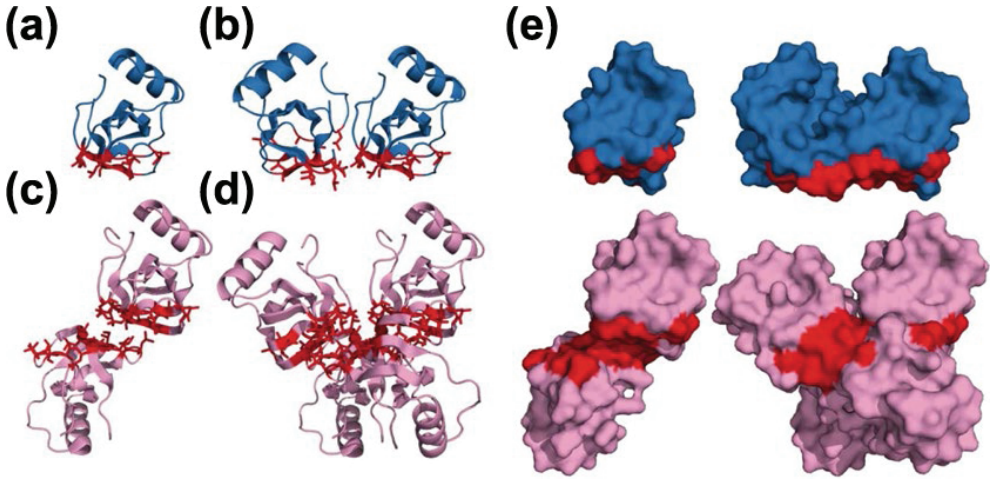

Figure 4 Oligomerization of HFBII. (a) A monomeric HFBII. (b) An amphiphilic dimer HFBII. (c) A hydrophilic dimer HFBII. (d) A loose, hydrophilic tetramer, composed of two dimers by symmetry relations. (e) A surface representation of structures (a)–(d). Reproduced with permission from Ref. [114], © The American Society for Biochemistry and Molecular Biology, Inc. 2007.

κ-casein, in an assumed weight ratio of 4:1:4:1 [117, 119]. The four components of caseins are all chain-like and self-assemblable. Due to the inhomogeneous distribution of polar and non-polar amino acids, they have obvious hydrophilic and hydrophobic domains [120, 121]. α_{S1}-Casein owns good self-assembling capacity, which can be adjusted by pH value and ionic strength. The self-assembling ability of α_{S2}-casein increases with the increment of ionic strength when the ion concentration does not exceed 0.2 M [122]. β-Casein can exhibit better self-assembly with increasing ionic strength and temperature in a suitable range [123, 124], and there is a concentration point that the self-assembly would be gradually enhanced until reaching the maximum [125]. Different from other caseins, κ-casein can form fixed-size polymers and not be affected by temperature and ionic strength in the proper condition. The parameters of pH, ionic strength, and temperature could be modulated to control drug release in casein-based drug carriers. Furthermore, caseins are proline-rich and presented as an open-structured form for the absence of α-helices and β-strands and –s–s– bridges. This flexible and unfolded property assures that caseins are quite thermostable, but can be easily degraded by proteases [126]. It has been reported that caseins could self-assemble into micelles with a radius of 50–500 nm, a mass of 10^3–3×10^6 kDa [126], and an inner cavity of 20–30 nm [127].

2.4 Self-assemblable artificial peptides

Self-assembly is a complex but ubiquitous natural phenomenon. The in-depth analysis of protein assembly and the rapid development of computer science have brought convenience to the artificial design of assemblable peptide modules.

2.4.1 Elastin-like polypeptide (ELP)

ELPs are a sort of artificial peptides typically consisting of pentapeptide motif $(VPGXG)_n$, in which X is a guest residue that represents any amino acid except proline for its existence at the fourth residue would interfere with coacervation and n is on behalf of the number of motif repeats. The design of ELP is inspired by the repetitive hydrophobic domain of human tropoelastin, which is a crucial component of elastic fibers and plays an important role in the stretching and recoil of certain organs and tissues [128–130].

As peptides with similar structure and function to elastin, ELPs composed of repeat motifs $(VPGXG)_n$ have unique temperature sensitivity [131, 132]. The peptide chains of ELPs are soluble at a temperature below inverse transition temperature (T_t), but are intertwined with each other to aggregate at a temperature above T_t [133–136]. A previous study demonstrated that the T_t of ELPs consisting of $(VPGXG)_n$ sequence can be customized by the substitution of amino acid X and altering the length of n [137]. By designing two types of repeat motifs with different T_t into one ELP chain, the ELP can be endowed with amphiphilicity to self-assemble into nanoparticles at a specific temperature range. For example, ELP containing $(VPGIG)_{48}(VPGSG)_{48}$ can form nanoparticle spontaneously, in which $(VPGIG)_{48}$ acts as a hydrophobic domain and $(VPGSG)_{48}$ acts as a hydrophilic motif [138].

2.4.2 Coiled-coil motif

Coiled-coils are composed of two or more α-helices that wind around each other in a supercoil. Coiled-coils exist in many proteins with significant biological functions, such as fibrin and transcription factor. The sequence of coiled-coil motifs usually contains a basic repeating seven-residue pattern with hydrophobic and polar residues. In the repeating pattern, the hydrophobic residues are conserved at the first and fourth position, and the other positions are commonly occupied by polar residues (*hpphppp*). Hydrophobic residues located at the interface between supercoiled α-helices are aligned to form a stable hydrophobic core while polar residues are located on the outside. To get better controllable self-assemblable coiled-coil structures, extending the hydrophobic residues beyond the first and fourth residues in repeating heptad pattern is feasible, such as *hpphpph*, *hpphhpp*, *hpphhph*, or *hphhphp* [139]. Liu et al. replaced fifth and seventh residues with nonpolar alanine in the GCN4 leucine zipper, and this mutant showed a stable α-helical heptamer formation [140]. Besides, coiled-coils of different sequences own unique structures, including a fiber (tropomyosin), a zipper (the Fos b-Zip domain), a tube (TolC), and a sheet (colicin IA) (Fig. 5(a)) [141]. What's more, the formation and dissociation of coiled-coil structures between polypeptide chains can be achieved by protonation/deprotonation of side-chain groups under different pH conditions. Klok and colleagues reported that peptides IAAL E3 (Ac-GYE-$(IAALEKE)_3$-IAALEKG-NH_2) and IAAL K3 (Ac-GYK-$(IAALKEK)_3$-IAALKEG-NH_2) could keep stable under neutral extracellular condition and dissociate in the late endosome (Fig. 5(b)) [142]. In recent years, coiled-coil motifs with different sequences have drawn attention for the construction of nanoassemblies with various morphology (Fig. 5(c)) [143–145]. Matrilin-1, a "cartilage matrix protein", is a central member of the human matriline family. The last 28 amino acids (Q466–T494) at its C-terminal could form a coiled-coil of four α-helices and

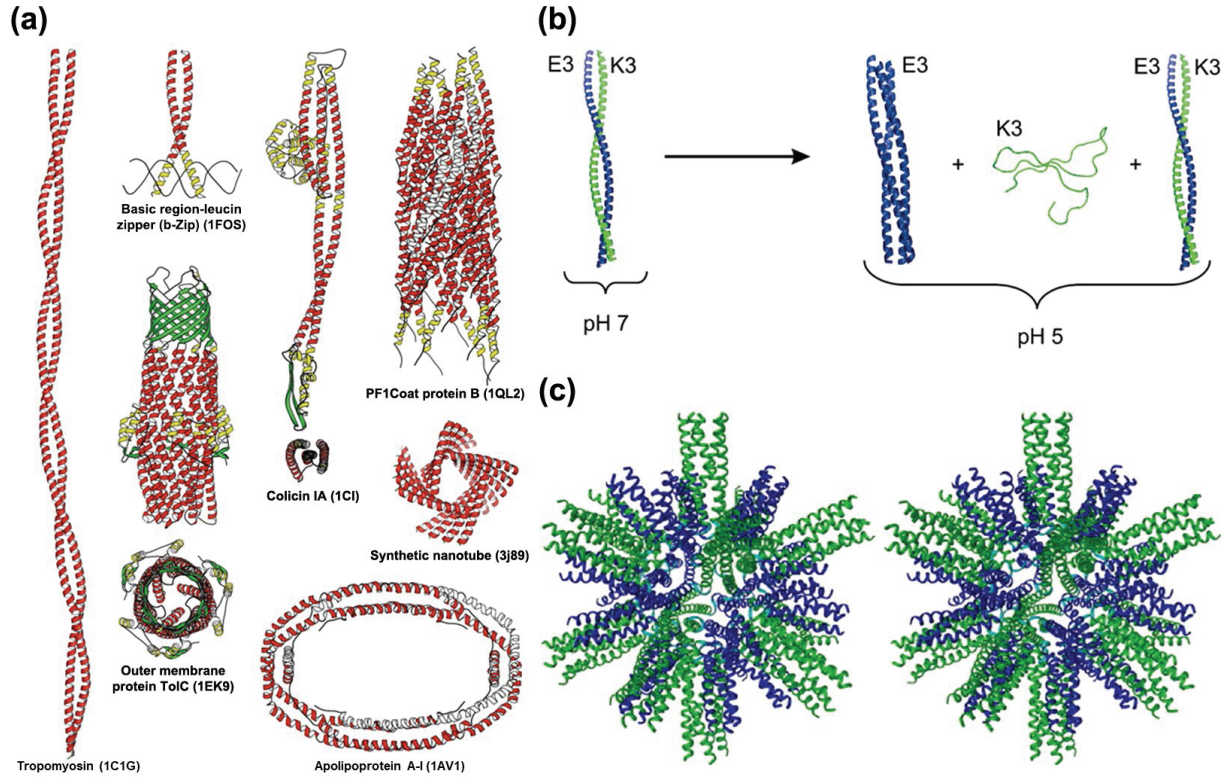

Figure 5 (a) Different structures of natural and synthetic coiled-coil motifs (reproduced with permission from Ref. [141], © Springer 2017). (b) The pH induced transformation of E3/K3 heterodimeric coiled-coil motifs (reproduced with permission from Ref. [142], © American Chemical Society 2008). (c) A computer model of the self-assembled peptide nanoparticles consisting of the pentameric coiled-coil domain of cartilage oligomerization matrix protein (green) and a trimeric *de novo* designed coiled-coil domain (blue) (reproduced with permission from Ref. [145], © Elsevier Inc. 2006).

assemble into a stable homodimer or trimer [146–149]. Burkhard and coworkers combined cartilage oligomerization matrix protein domain with a designed minimal trimeric coiled-coil domain via two glycine residues to form a nanoparticle consisting of 60 monomeric building blocks with a regular polyhedral symmetry [145]. Eriksson et al. applied right-handed coiled-coil (RHCC) peptides from archaebacterium *Staphylothermus marinus* to envelope cisplatin into RHCC's hydrophobic cavities by simply mixing and stirring at room temperature [150].

2.4.3 *De novo designed peptide*

In addition, a number of peptides with simple sequence and assemblable capability have been designed to construct nanoassemblies [151]. Theoretically, the designed peptide sequences can be diverse and the driving force of self-assembly can also be complex, but the most commonly reported self-assembly peptides are amphiphilic with the hydrophobic portion aggregating inside the nanoparticle, while the hydrophilic portion distributes toward the outer aqueous phase. For instance, Zhou and coworkers designed a series of diblock poly(lysine-β-phenylalanine) copolypeptide with polar lysine and nonpolar phenylalanine [152]. Chen and coworkers designed a amphiphilic peptide sequence HFFHGHFFHGHFFHGKK to encapsulate water-insoluble drug lonidamine [153]. Sigg et al. synthesized a reduction-responsive amphiphilic peptide consisting of histidine, tryptophan, and reductive linker, which could self-assemble to load doxorubicin (DOX) and antisense oligonucleotides Atto550 simultaneously [154].

Since the electrostatic interaction influential on the self-assembled architectures tends to be pH-regulated, the design of pH-responsive peptides is a feasible and simple approach for controlled drug release. Gong et al. used lysine as the hydrophilic part and isoleucine as the hydrophobic part to constitute I_6K_5, a pH-responsive cationic peptide, which could form nanoparticles at a neutral pH value and disassemble in an acidic environment [155]. The nanoparticle assembled from amphiphilic peptide LLLLLLKKKGRGDS also showed pH-responsive property [156].

3 Application of protein/peptide-based nanoassemblies for drug delivery

Nanoassemblies have shown extraordinary performance in the design of drug carriers to overcome issues such as low solubility and poor stability of drugs. Moreover, it is known that the therapeutic efficacy of drug-loaded nanoassemblies ultimately depends on their ability to reach the target of action. From administration site to diseased tissue, drug-loaded nanoassemblies go through a complex journey in the body. Multiple factors including circulation time, physiology barrier, targeting efficiency, and controlled release all significantly affect delivery efficiency. In this section, we outline protein/peptide-based nanoassemblies with distinct functionalities for improved efficacies and reduced side effects (Table 1).

3.1 Passive targeting

The term "passive targeting" refers to the phenomenon of involuntary distribution to specific tissues, organs, and cells by adjusting the size, morphology, and surface properties of the carriers. Passive targeting has been widely used to describe the findings of the enhanced accumulation of nanoparticles in solid tumors with leaky vasculature and compromised lymphatic drainage. This enhanced permeability and retention (EPR) effect has been found on different types of nanocarriers with the size ranging from 20 to 350 nm [157–161].

Huang et al. chemically conjugated indocyanine green dye (IR820) to the ELP chain ($[V_1G_7A_8$-32]/[VH_4-40]) and constructed IR820-ELP/Zn^{2+} chelation with a size of 55 nm [162]. On the CT-26-bearing mice model, intravenous injection of IR820-

Table 1 Summary of protein/peptide-based nanoparticles for drug delivery

Strategy	Carrier	Modified group	Cargo	Disease model	Ref.
Passive targeting	ELP[$V_1G_7A_8$-32]/[VH_4-40]	/	Indocyanine green dye IR820	CT-26 cells	[162]
	ELP[$G(VPGSG)_{48}$ $(VPGIG)_{48}Y$]	FKBP	Rapamycin	MDA-MB-468 cells	[138]
Active targeting	HFBI	RGD peptide	BODIPY derivative	U87-MG, HeLa, and MCF-7	[166]
	HAVRNGRRGDGGAVPIAQ K (HRK-19)	/	DOC	A549 cells	[167]
	VLP from MrNV	FA	DOX	HT29 and HepG2 cells	[173]
	Fn	A specific collagen II-targeting peptide	HCQ	Osteoarthritis	[174]
	Fn	An extracellular-signal-regulated kinase (ERK)peptide inhibitor	PTX	MDA-MB-231 and A549 cells	[177]
Long circulation	VLP from PhMV	PEG	DOX-EMCH	MDA-MB-231 cells	[180]
	Fn	An ABD variant	DOX	A549 cells	[181]
	HFn	BCP1 (CNARGDMHC)	DOX	B16 cells	[182]
BBB transport	Qβ-based VLP	Apolipoprotein E peptide (ApoEP), cell penetrating peptide (CPP)	Luciferase mRNA and c-MET mRNA	U87 cells	[187]
	Fn	/	Cy5 and PTX	Bend.3 and C6 cells	[188]
	Fn	/	IRdye800 and DOX	U87-MG cells	[68]
	HFn	Integrin $\alpha_2\beta_1$ targeted ligand (DGEAGGDGEA)	DOX	U87-MG cells	[189]
	Fn	/	Fe_3O_4 nanozyme	Cerebral malaria	[190]
pH-responsive release	HFn	Dual-functional carbon dots	DOX	MCF-7 and S180 cells	[193]
	A cationic peptide I_6K_5	/	DOX	Bel-7402 cells	[155]
	smHSPs	/	DOX	/	[81]
Reduction-responsive release	HFBII	/	Dodecanethiol-modified gold nanoparticles and PTX	HeLa, MG-63, U87-MG, MDA-MB-231, and 4T1 cells	[116]
	VLP from JCV	Mono-2-O-(p-toluenesulfonyl)-β-cyclodextrin	PTX, RA	NIH3T3 cells	[194]
	VLP from CPMV	/	DOX	HeLa cells	[195]

ELP/Zn^{2+} nanoparticles showed more accumulation at the tumor sites because of the EPR effect compared to free IR820. Dhandhukia et al. fused ELP chain ($G(VPGSG)_{48}(VPGIG)_{48}Y$, abbreviated as SI) with FK-506 binding protein 12 (FKBP) to obtain FSI fusion peptide for the encapsulation of rapamycin (Rapa) [138]. On the MDA-MB-468 tumor-bearing mice, the group receiving intravenous injection of FSI-Rapa exhibited dramatically enhanced tumor inhibition compared with the free Rapa group.

3.2 Active targeting

In comparison with passive targeting, nanoparticles modified with targeting ligands as "missiles" delivering drugs to the target area are called active targeting preparations. Studies have shown that the occurrence and development of diseases are often accompanied by the abnormal expression of specific receptors on the cell surface. Therefore, targeting ligands that can recognize and bind to the overexpressed receptors on cell membrane have been exploited to arm nanoparticles for improved targeting efficiency [163–165].

Xiao et al. used RGD-HFBI fusion protein to encapsulate near-infrared (NIR) fluorescent probe, boron-dipyrromethene (BODIPY), for solubilization and tumor active targeting [166]. Cell uptake assay demonstrated that RGD-HFBI-coated BODIPY could stain $\alpha v\beta_3$ integrin-positive cancer cells (U87-MG) more efficiently than HFBI-coated BODIPY and free BODIPY, while no distinctive difference was observed between the groups on $\alpha v\beta_3$ integrin-negative MCF cells. Besides, due to the targeting ability of the RGD, RGD-HFBI/BODIPY could be imaged at the tumor site for 72 h after administration, while HFBI/BODIPY only remained for 48 h in the U87-MG-bearing mice as shown in the *in vivo* imaging study.

Guo and coworkers reported that self-assembled nanocarriers based on HAVRNGRRGDGGAVPIAQK (HRK-19) peptides displayed prominent tumor-targeted properties (Fig. 6(a)) [167]. In addition to the RGD targeting ligand, the NGR peptide motif was designed in the sequence to recognize the tumor vascular antigen CD13 associated with tumor angiogenesis [168–170]. HAV peptide motif, a highly conserved sequence at classical cadherin homophilic binding site, can inhibit cell aggregation, compaction, and neurite outgrowth. The formed nanoparticles owned a spherical structure with a size of about 62 nm. On the A549-bearing mice model, docetaxel (DOC)-loaded HRK-19 nanoparticles (DOC/peptide)-treated groups showed significantly lower tumor weight and longer median survival than that of the free Taxotere group. *In vivo* imaging study showed that the fluorescent dye DiD loaded HRK-19 nanoparticles accumulated more effectively in the tumor site than the free DiD solution. Folic acid (FA) is another commonly used ligand to target malignant tumors that overexpress folate receptors [171, 172]. Tan and coworkers modified FA onto the VLP derived from MrNV to load DOX (FA-MrNVLP-DOX) for anticancer therapy [173]. Enhanced cellular uptake and cytotoxicity of FA-MrNVLP-DOX were observed on HT29 cells compared to DOX-loaded VLP and free DOX groups.

For osteoarthritis therapy and imaging, Chen et al. constructed

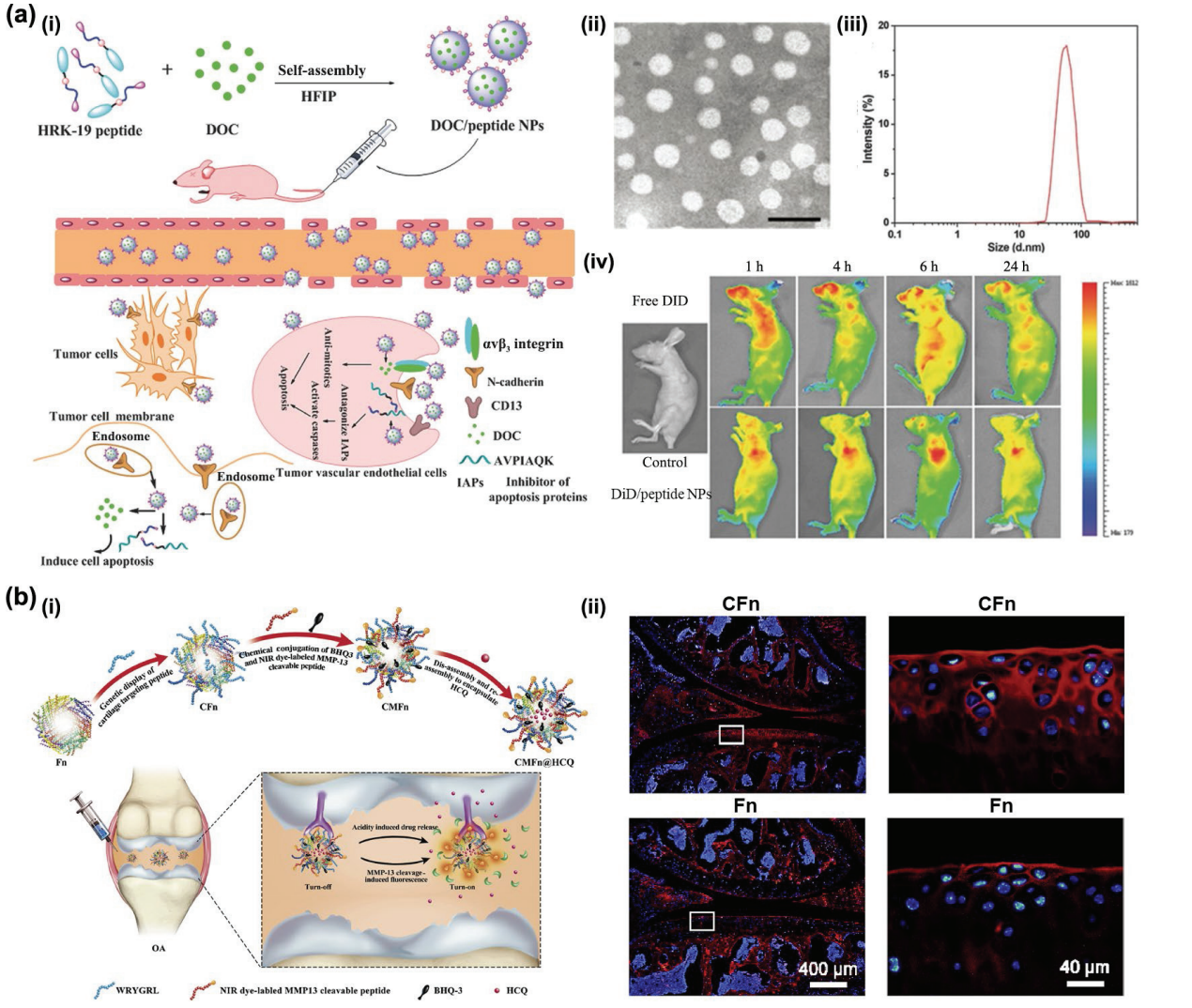

Figure 6 (a) DOC/peptide nanoparticles for pulmonary carcinoma therapy. (i) Schematic illustration of assembly mechanism and tumor targeting of DOC/peptide nanoparticles. (ii) TEM image and (iii) particle size distribution of DOC/peptide nanoparticles. (iv) *In vivo* images of A549-bearing mice after treatment with free fluorescent dye DiD or DiD/peptide NPs for different time points. Reproduced with permission from Ref. [167], © Fan, R. R. et al. 2017. (b) Functional Fn nanocage as targeted drug delivery vehicles for osteoarthritis treatment. (i) Schematic illustration of the CMFn@HCQ for imaging and precision therapy of osteoarthritis. (ii) Penetration of CFn and Fn into cartilage for 24 h after incubation at 37 °C. Reproduced with permission from Ref. [174], © Elsevier Ltd. 2019.

collagen II-targeting peptide modified Fn-based nanocage to load anti-inflammatory drug hydroxychloroquine (HCQ), NIR dye (cy5.5)-labeled MMP13 cleavable peptide, and a quencher BHQ-3 to obtain CMFn@HCQ (Fig. 6(b)) [174]. Peptide WRYGRL capable of targeting collagen II, the major component of the cartilage matrix, was genetically modified onto the Fn-based nanocage. *In vivo* imaging study showed that CMFn group owned better immobilization in the knees than that of MFn group without targeting peptides. Besides, penetration of cartilage-targeting CFn in the matrix compartment and within chondrocytes was more efficient than Fn only, which confirmed the cartilage-targeting capability of peptide WRYGRL.

Bare HFn nanoparticles can also be classified into active targeting preparations since Fn-based nanocage can target tumor cells with overexpressed TfR1 and then enter cells through receptor-mediated endocytosis [175, 176]. Zhang and coworkers utilized the Fn-based nanocage to deliver PTX by genetically modifying an extracellular-signal-regulated kinase (ERK) peptide inhibitor (MPKKKPTPIQLNP) on its C-terminal of Fn, named HERK [177]. The ERK peptide inhibitor was able to induce cell apoptosis by disrupting the MAPK/ERK pathway and killing tumor cells in combination with PTX. *In vitro* experiment showed that when treated to the TfR1 expressed MDA-MB-231 and A549 cells, FITC-labeled HERK showed a higher uptake effect than free FITC, but the uptake would be almost inhibited after pre-incubation Fn with tumor cells, indicating that HERK can enter tumor cells through TfR1-mediated endocytosis. With the low pH-mediated decomposition of HERK in the lysosome, PTX was released from the nanocage and exerted a synergistic anti-tumor effect with the ERK inhibitor.

3.3 Long circulation

As a "protective umbrella" for drugs against the physiological environment, nanocarriers are believed to improve the stability and targeting of laden drugs, leading to significant clinical advantages. However, the clinical application of nanoparticles is commonly limited because of the quick clearance *in vivo*. As increased blood circulation time of administered nanoparticles can improve the efficiency of tumor targeting, it is desirable to develop long circulation strategies with clinical application potential.

The introduction of polyethylene glycol (PEG) shells on the outer surface of nanoparticles has been shown to effectively avoid reticuloendothelial systems *in vivo* and prolong the duration of the systemic circulation [178, 179]. Hu and Steinmetz modified PEG onto the external surface of PhMV-based VLP to load DOX (DOX-PhMV-PEG) for longer circulation and less nonspecific

cellular uptake [180]. On the MDA-MB-231 xenograft mice model, compared to free DOX, administration of DOX-PhMV-PEG showed significantly enhanced antitumor efficacy with the rate of complete tumor clearance high to 80% during the study period.

Wang et al. fused an albumin binding domain (ABD) onto HFn and constructed ABD-HFn nanoparticles to load DOX for prolonged half-life (Fig. 7(a)) [181]. ABD displays extremely high affinity to HSA in the subnanomolar range. The binding of ABD-HFn to HSA increased the diameter of nanoparticles from 12 to nearly 30 nm to avoid rapid renal clearance [181]. In addition, the increased steric hindrance of HSA binding on the surface of nanoparticles could decrease TfR1-mediated cell uptake and endocytosis. The pharmacokinetic parameters in Sprague Dawley (SD) rats showed that the apparent blood half-life and area under the curve (AUC) value of ABD-HFn/DOX nanoparticles were both about 12 times that of HFn/DOX nanoparticles.

Jin et al. integrated a blood circulation prolonging (BCP) peptide from a peptide of phage to HFn through genetic engineering for tumor-targeted delivery of DOX (Fig. 7(b)) [182]. The BCP peptide (CNARGDMHC) containing the RGD motif can target tumor cells and bind to platelets for longer blood circulation. Both in the cell and animal study, DOX-loaded BCP-modified HFn nanoassemblies (BHFn-DOX) showed an enhanced tumor-killing effect than HFn-DOX without BCP modification and free DOX group. In the pharmacokinetic study, the half-life of BHFn-DOX was longer than that of HFn/DOX, and AUC and maximum concentration (C_{max}) of BHFn-DOX were higher than those of HFn-DOX, indicating that BCP1 peptide could dramatically increase the blood circulation time of DOX.

3.4 BBB transport

The BBB is a protective barrier in the body, consisting of tight junctions of capillary endothelial cells on one side and foot processes of astrocytes on the other side. The BBB plays a key role in protecting the central nervous system from toxic and infectious pathogens, but also hinders the brain delivery of drugs [183]. Usually, only lipophilic molecules with a molecular weight of less than 400–600 Da can transport across the BBB.

Receptor-mediated transcytosis is an effective strategy to deliver drugs across the BBB [184–186]. As low-density lipoprotein receptors are highly expressed on the surface of cerebral endothelial blood vessels, low-density lipoprotein can be modified onto the nanoparticles to mediate brain targeted delivery. Pang et al. constructed apolipoprotein E peptide (ApoEP) and cell-penetrating peptide (CPP) dual modified Qβ-based VLPs for brain delivery of designed RNAi (c-MET) to reduce the invasion and migration of tumor cells (Fig. 8(a)) [187]. Green fluorescent protein (GFP) or mCherry protein was fused with Qβ coat proteins as luminophore for observation. On intracranial U87-bearing mice, the CPP and ApoEP modified mCherry protein-fused VLP/RNAi$_{c\text{-}MET}$ (dP@mVLP/RNAi$_{c\text{-}MET}$) treated group showed numerous stained mCherry protein signals in the brain, particularly in the tumor tissues than the group without the CPP and ApoEP modification (mVLP/RNAi$_{c\text{-}MET}$). In the anticancer study, the combined administration of temozolomide (TMZ) and gVLP/RNAi$_{c\text{-}MET}$ extended the median survival time of mice to 42 days, significantly longer than 25 days of the TMZ-only group, indicating that the designed nanocomposite can successfully reach brain tumors and reverse the resistance of TMZ.

Since TfR1 is not only expressed on the tumor cells but also the endothelial cells of the BBB, Fn-based nanoassemblies can effectively cross the BBB via transferrin receptor-mediated transcytosis. Liu et al. employed HFn to load PTX for the treatment of brain malignancy [188]. The cellular uptake of Cy5-loaded HFn was much higher on Bend.3 and C6 cells than that of free Cy5, which could be competitively inhibited by the co-incubation with anti-TfR1. On intracranial C6-bearing mice, the HFn-Cy5 treated group exhibited stronger fluorescence around the brain region than the free Cy5 treated group, suggesting that HFn are capable of transporting across the BBB and accumulating in the brain area. In the tissue distribution study, large amounts of PTX delivered by HFn accumulated in the brain while free PTX could hardly permeate the BBB and aggregate in the brain area.

Yan and colleagues systemically compared the BBB transcytosis ability of Fn nanocages composed of the L-chain and H-chain, respectively (Fig. 8(b)) [68]. The *in vitro* biomimetic BBB experiment showed that the transport rate of HFn was more than 5 times higher than that of L-chain Fn (LFn). The results of the *in vivo* BBB penetration ability showed that the fluorescence of IRdye800-HFn was more concentrated in the brain area than in other organs on the healthy mice. In addition, on the orthotopic glioma mice, IRdye800-HFn further accumulated at the tumor site after crossing the BBB, whereas IRdye800-LFn presented much less signal in the brain and glioma, leading to the conclusion that HFn is superior to LFn in BBB transcytosis.

Huang and coworkers fused HFn with integrin $\alpha_2\beta_1$-targeting ligand (DGEAGGDGEA) through genetic engineering to obtain 2D-HFn fusion protein and constructed DOX-loaded 2D-HFn nanocage to target glioblastoma with up-regulation of integrin $\alpha_2\beta_1$ [189]. The *in vitro* study showed that the permeation

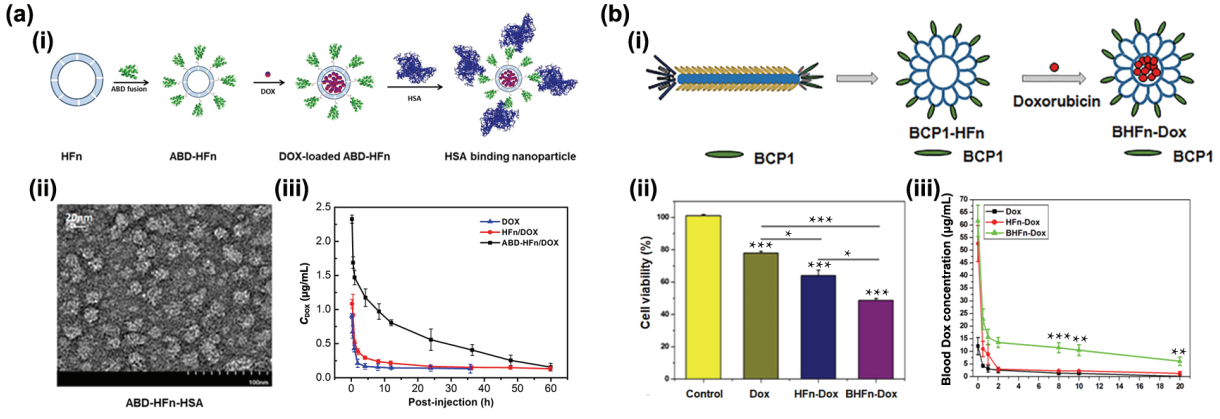

Figure 7 (a) ABD-fused HFn nanocage for prolonged *in vivo* circulation of DOX. (i) Schematic design of the construction of ABD-HFn/DOX nanoparticles. (ii) Morphological observation of saturated HSA binding ABD-HFn nanoparticles by TEM. (iii) Pharmacokinetics study of DOX, HFn/DOX, and ABD-HFn/DOX in SD rats. Reproduced with permission from Ref. [181], © American Chemical Society 2018. (b) BCP1 peptide modified HFn to load DOX for anticancer therapy. (i) Schematic design of the formation of BHFn-DOX nanoparticle. (ii) Viability of B16 cells treated with PBS, DOX, HFn-DOX, or BHFn-DOX for 24 h. (iii) Blood DOX concentration versus time after mice receiving DOX, HFn-DOX, or BHFn-DOX. Reproduced with permission from Ref. [182], © American Chemical Society 2019.

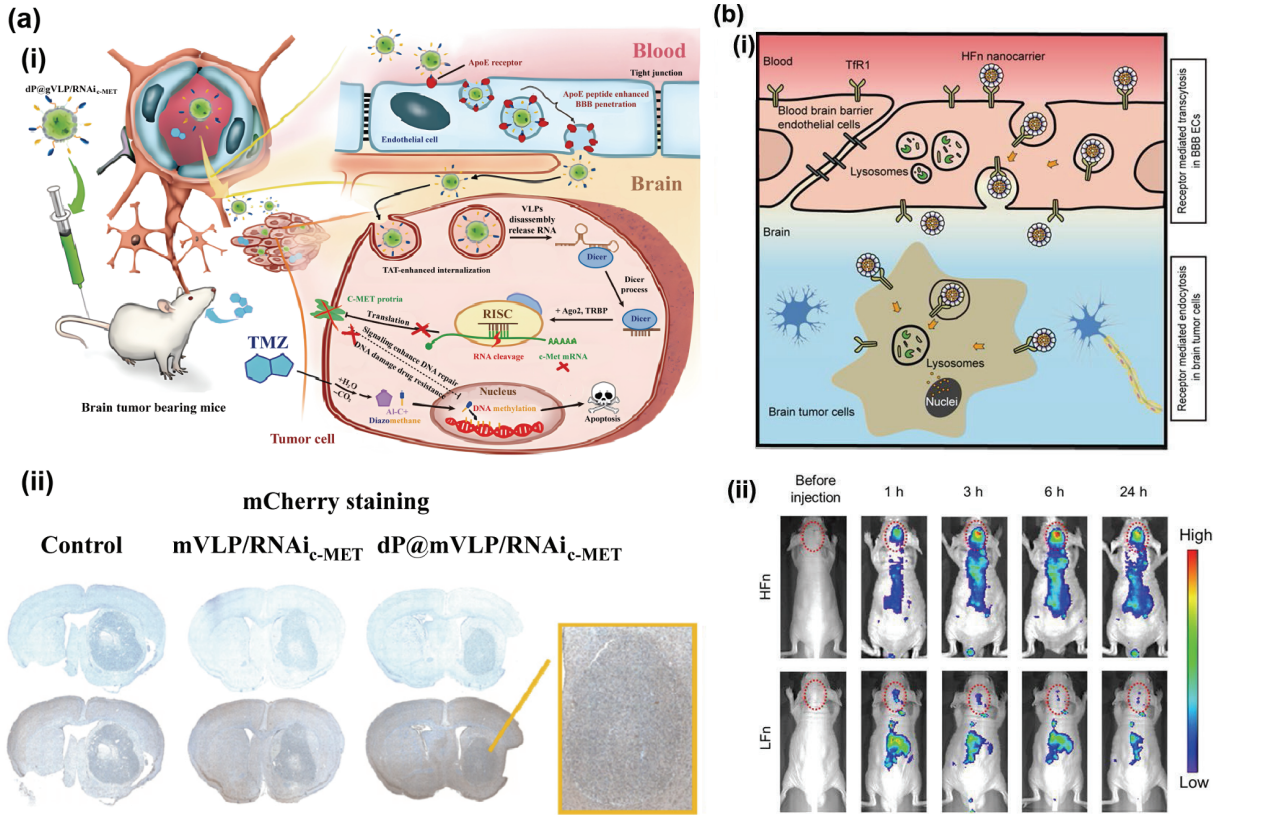

Figure 8 (a) Dual-functional modified Qβ-derived VLP for brain drug delivery. (i) Scheme of BBB penetration and subcellular delivery of dP@gVLP/RNAi$_{c\text{-}MET}$. (ii) mCherry staining sections of mouse brains. Reproduced with permission from Ref. [187], © The Royal Society of Chemistry 2019. (b) TfR1 mediated brain-targeted delivery of HFn nanocage. (i) Scheme of BBB transport and tumor-targeted delivery of HFn nanocarrier. (ii) *In vivo* imaging of IRdye800-HFn and IRdye800-LFn on the orthotopic U87-MG-bearing mice after intravenously injection. Reproduced with permission from Ref. [68], © American Chemical Society 2018.

efficiency of FITC-loaded 2D-HFn through biomimetic BBB was 59.2%, significantly higher than 29.4% of FITC loaded HFn and 0.1% of free FITC. On the U87-MG xenograft mice models, the intravenous injection of IRDye-800-loaded 2D-HFn was able to cross the BBB and accurately bound to the tumor lesion in the brain with a high tumor-to-normal tissue ratio of 2.

Zhao et al. developed an Fn nanozyme (Fenozyme) consisting of a human Fn shell and Fe_3O_4 nanozyme inner core for the treatment of cerebral malaria [190]. The Fn shell promotes the brain delivery of Fe_3O_4 nanozyme which then exhibits catalase-like activity to inhibit the high level of reactive oxygen species (ROS). On the cerebral malaria-bearing mice, Fenozyme could protect the BBB endothelial cells from ROS damage and decrease parasite-infected red blood cells. 80% of the cerebral malaria-infected mice treated with phosphate buffered saline (PBS) or blank HFn nanoparticles were unable to survive 10 days, whereas only 20 % of them died by day 16 after receiving 3.75 mg/kg of Fenozyme. Furthermore, the combination of Fenozyme and anti-malaria artemether enabled to alleviate encephalopathy and memory impairment on the mice that survived cerebral malaria.

3.5 Stimuli-triggered controlled release

Variations of parameters in physiological or pathological environments, such as pH value, redox balance, and enzyme levels, provide the possibility for precise and controlled release of therapeutics. Recently, with the exploration of intelligent materials that can respond to small changes in physical or chemical conditions with a relatively large change in property, the development of stimuli-responsive drug delivery systems has been rapidly expanded [191, 192].

3.5.1 pH-responsive drug release

Fn, as a type of ideal material for the construction of pH-sensitive carriers, can self-assemble in a neutral environment and disassemble under low-pH condition. Yao et al. employed HFn to encapsulate DOX and modify carbon dots (CDs) to the surface of HFn to obtain pH-responsive nanoassembly HFn(DOX)/CD for imaging and combination antitumor effect (Fig. 9(a)) [193]. The nanoassembly HFn(DOX)/CD released 77.8% DOX at pH 5.0, significantly higher than 28.7% at pH 7.4, suggesting that HFn(DOX)/CD can effectively respond to the acidic environment of endosomes/lysosomes for accelerated drug release.

Bai and coworkers reported a cationic peptide IIIIIIKKKKK (I_6K_5) with pH-responsive property for the delivery of DOX (Fig. 9(b)) [155]. The self-assembled I_6K_5-based nanoparticles were spherical with a diameter of around 30 nm at pH 7.4. In comparison, the intact shape of nanostructures became swollen and irregular as a large portion of random coil structures formed after incubating at pH 6.0. The variation of morphology resulted in an excellent pH-responsive release of DOX-loaded I_6K_5 nanoparticles.

Another strategy is to modify the drug onto the nanocarrier via pH-sensitive bonds. Flenniken et al. chemically conjugated DOX onto smHSPs with an acidic labile hydrazone linker for controlled release [81]. Cysteine residues mutated on the interior surface of smHSPG14C carriers can selectively react with (6-maleimidocaproyl) hydrazone of DOX derivation (Fig. 9(c)). The releasing experiment showed that incubating at different pH values of 4.0, 4.5, and 5.0, the time for releasing 50% of DOX from smHSPG14C nanocarriers through hydrolyzing the hydrazone linkage was 1.5, 3.9, and 5.1 h, respectively, indicating the acidic microenvironment of lysosome could promote the release of DOX.

3.5.2 Reduction-responsive drug release

Protein-based nanoassemblies with disulfide bonds are considered

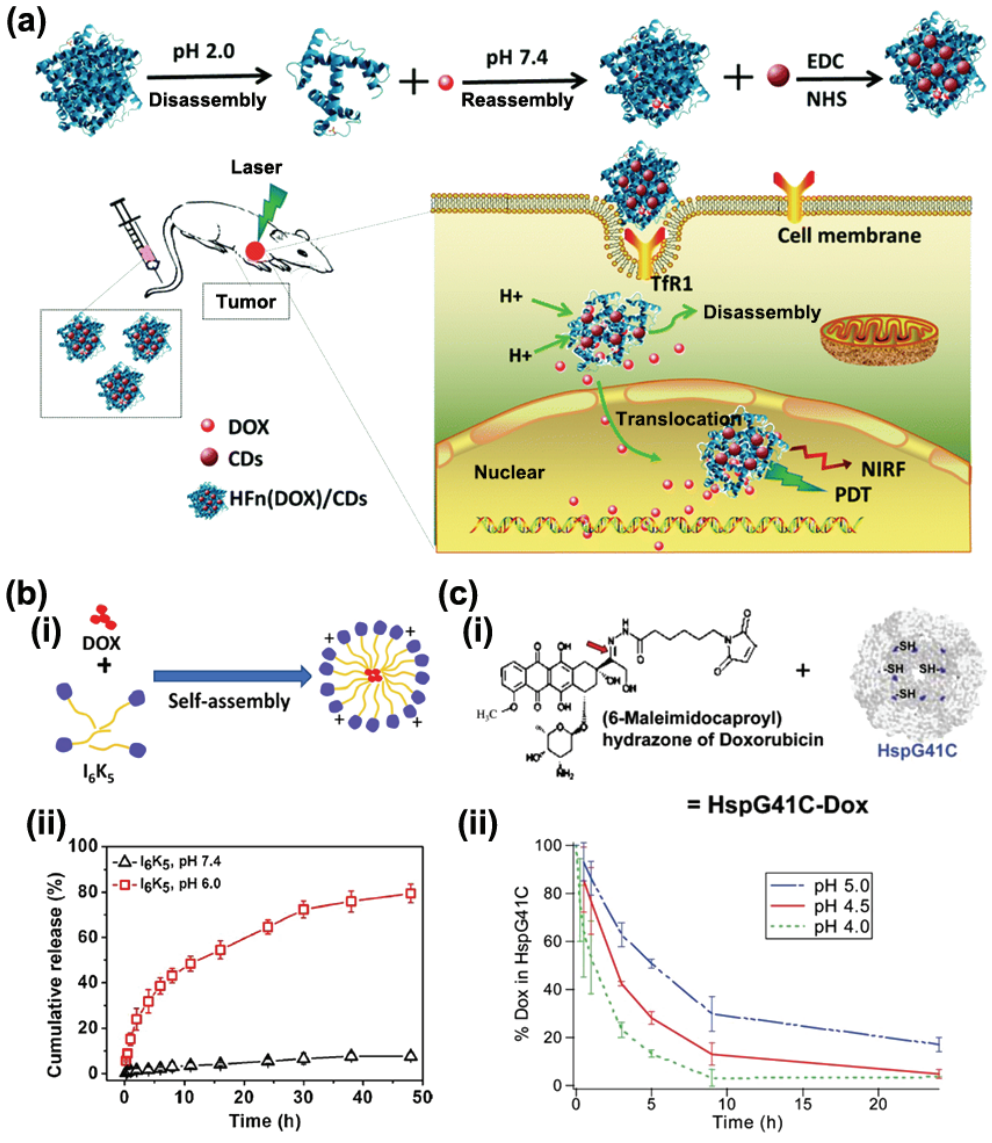

Figure 9 (a) Schematic illustration of the principle of drug loading and nuclear targeting of HFn(DOX)/CDs (reproduced with permission from Ref. [193], © The Royal Society of Chemistry 2018). (b) pH-triggered drug release of DOX-loaded I_6K_5 nanoparticles. (i) Schematic illustration of the self-assembly of cationic peptide I_6K_5 for the encapsulation of DOX. (ii) The release profile of DOX from I_6K_5 nanoparticle at different pH values. Reproduced with permission from Ref. [155], © Elsevier 2020. (c) pH-mediated drug release of HSPG14C nanoassembly. (i) Reaction scheme showing the conjugation of the (6-maleimidocaproyl) hydrazone of DOX to the HSPG14C cage. (ii) pH-triggered release of DOX from HSPG14C cages. Reproduced with permission from Ref. [81], © The Royal Society of Chemistry 2005.

intrinsic reduction-responsive carriers. Maiolo et al. reported bioreducible HFBII-stabilized supraparticles consisting of HFBII and gold nanoparticles (AuNPs) for selective intracellular release [116]. The modification of dodecanethiol (DT) on the surface of AuNPs acted as a hydrophobic surface, which enabled HFBII to encapsulate AuNPs into their hydrophobic cores via non-covalent interactions (Fig. 10(a)). Transmission electron microscopy (TEM) observation showed the presence of spherical-like supraparticles with a diameter of around 30 nm. The supraparticles were stable in plasma and exhibited a slow release profile of loaded hydrophobic molecules, which was possibly ascribed to the coating of impermeable and rigid HFBII film. On the other hand, disulfide-rich HFBII can change the secondary structure in response to high intracellular glutathione (GSH) concentration of 5–10 mM, leading to the dismantling of the HFBII membrane and the sudden release of the encapsulated drugs. The cytotoxicity study showed that compared to free PTX, PTX-loaded supraparticles (SP@PTX) owned 1 or 2 orders of magnitude reduction of the drug half-maximal inhibitory concentration (IC_{50}) on PTX-sensitive (HeLa, MDA-MB-231) and PTX-resistant (4T1) cancer cells.

Another approach is to conjugate drugs onto nanocarriers via disulfide bond to achieve reduction-responsive release. Niikura et al. conjugated thiosulfate containing β-cyclodextrin (-ss-CD) with cysteine group on the inner cavity of human JC polyomavirus (JCV) derived VLP to obtain VLP–CD by the formation of a disulfide bond [194]. Hydrophobic drug PTX and fluorescent compound rhodamine-linked adamantane (RA) were included in CD to form VLP–CD–PTX and VLP–CD–RA, respectively (Fig. 10(b)). In the release experiment, small amounts of RA were released from VLP–CD–RA in the buffer with a low concentration of GSH (10 μM), while a mass of RA released from VLP–CD–RA were detected in a short time with a high concentration of GSH (10 mM). The nanocarrier could facilitate the cellular uptake of PTX into NIH3T3 cells and release PTX efficiently in the cancer cells with a high level of GSH, resulting in higher cytotoxic activity compared to free PTX. Aljabali et al. conjugated DOX onto VLP from CPMV through a disulfide bond to obtain CPMV-SS-DOX nanoparticles for anticancer treatment [195]. In the cytotoxicity study, CPMV-SS-DOX showed higher tumor cell killing effect on HeLa cells than CPMV-DOX nanoparticles without disulfide bond, indicating that the effective

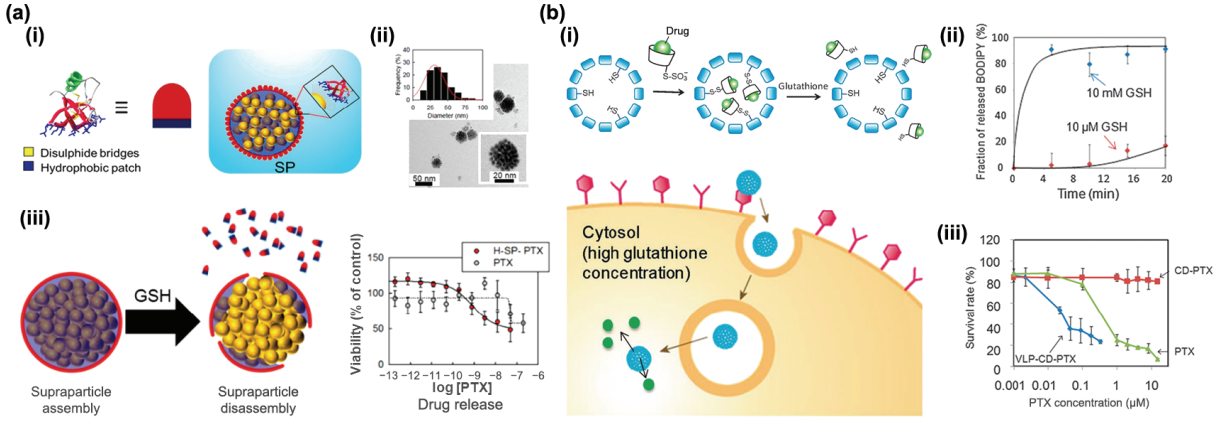

Figure 10 (a) Reduction-responsive HFBII-based superpaticles for controlled drug release. (i) HFBII molecular structure model derived from the PDB file 2B97 (left) and its solubilization for hydrophobic AuNPs (right). (ii) TEM image of HFBII-based nanoparticles with the corresponding size distribution. (iii) The HFBII-based superpaticles can be disrupted by GSH. Cytotoxicity study of different formulations on MDA-MB-231 cells. Reproduced with permission from Ref. [116], © American Chemical Society 2017. (b) VLP connected with thiosulfate containing β-cyclodextrin for reduction-responsive drug release. (i) Schematic illustration of the construction of VLP-CD-PTX and reduction-triggered release in tumor cells. (ii) Release study of BODIPY from the nanocage with different GSH concentrations. (iii) Cytotoxic study of different formulations on NIH3T3 cells. Reproduced with permission from Ref. [194], © The Royal Society of Chemistry 2013.

release of DOX upon the cleavage of disulfide bond by GSH in cancer cells resulted in significant cytotoxicity.

4 Application of protein/peptide-based nanoassemblies for vaccine development

The incorporation of nanomedicine with vaccines has been extensively implemented for enhanced treatment outcomes. In this section, we outline emerging advances in the use of protein/peptide-based nanoassemblies in vaccine development.

In vaccinology, nanoparticles mainly serve as adjuvants, carriers, or presentation platforms to improve the immune response through one or a combination of these roles [196]. In addition to improving stability and avoiding degradation, protein/peptide-based assemblies with a diameter between 20–200 nm enable to promote uptake by antigen-presenting cells (APCs) and retention in lymph nodes. Another advantage is that the ordered arrangement of antigens on the surface of nanoassemblies facilitates B-cell activation by crosslinking multiple B-cell receptors. Taken together, these factors result in a significant augment of immune response.

As the first commercially approved protein-based vaccine platform, VLP that mimics the size and geometry of virus has drawn continuous attention. VLP assembled from capsid proteins without the genome can be engineered to convey antigenic epitopes from either parental or exogenous virus. There are increasing fundamental, preclinical, and clinical studies that focus on the VLP vaccine for the prevention of different infectious diseases covering coronavirus disease 2019 (COVID-19) [197], seasonal influenza [198], malaria [199], and influenza (H5N1, H1N1 virus) [200–202]. Ortega-Rivera et al. selected CCMV and Qβ-based VLPs to carry three different target epitopes (570, 636, and 826) from SARS-CoV-2 S protein to build VLP-based vaccines against COVID-19 [203]. These designed vaccines could efficiently activate B cells and induce them to produce the opsonizing antibody IgG2a/b. Christiansen et al. used quadrivalent genotype hepatitis C virus (HCV) VLP vaccines produced in the lab to load antigenic domain B and D epitopes of the E2 protein, which could stimulate strong immunogenicity and genotype memory B cells without adjuvant [204]. Bachmann and coworkers found that *E. coli*-derived mRNA-loaded VLP was able to induce the activation of B cells and differentiate them into plasma cells, resulting in a quick onset of strong humoral IgG response [205]. Numerous investigations indicated that the rigid and repetitive surface structures of VLPs render them highly immunogenicity via facilitating cross-linking of B cell receptors. Moreover, the unique structure of VLPs promotes the binding with multimeric ingredients in the immune system, leading to effective opsonization, improved uptake of APCs, and thus enhanced immune responses [206].

Fn and other nanoassemblies with ordered and repetitive subunit structure have also emerged as promising antigen presentation platforms in recent years. Kanekiyo et al. introduced the trimeric haemagglutinin into the 3-fold axis of the Fn-based nanoassembly through genetic engineering for reciprocal stabilization, which was beneficial to the oligomerization of conformation-dependent trimeric antigens [207]. Compared with the licensed inactivated vaccine, Fn-based nanoassembly enhanced the immunological potency, which elicited over 10-fold higher antibody titers in immunized mice.

Kang et al. applied spike protein receptor-binding domain (RBD) as an antigen to prepare three vaccine candidates based on various nanoassemblis, RBD-Ferritin (24-mer), RBD-mi3 (60-mer), and RBD-I53–50 (120-mer) (Fig. 11(a)) [208]. mi3 protein that was computationally designed based on KDPG aldolase could self-assemble into a dodecameric cage scaffold with 60 total subunits and multiple display positions on the surface [209, 210]. The I53–50 NPs were an icosahedral nanoparticle assembled from two components, 20 copies of trimeric I53–50A.1PT1 and 12 copies of pentameric I53–50B.4PT1 [211]. All of three vaccine nanoassemblies were produced through SpyTag/SpyCather conjugation strategy, and the particle sizes of RBD-Ferritin, RBD-mi3 and RBD-I53–50 nanoparticles were about 33, 55, and 51 nm respectively. When immunizing the mice with RBD-Ferritin, RBD-mi3, or RBD-I53–50 with adjuvants, 71.8- to 168.4-fold higher binding antibody response was detected compared to the RBD only group. In addition, the neutralization activities of sera from three different nanoassemblies were nearly 10-fold higher than those of the RBD monomer group. In general, the RBD-conjugated nanoassemblies showed dramatically stronger immunization efficacies than the RBD monomer.

Babapoor et al. designed two types of assemblable peptides Mono-M2e and Tetra-M2e by fusing coiled-coil motifs with the external domain of matrix protein 2 (M2e) for the construction of universal avian influenza (AI) vaccines [212]. M2e exists on the surface of Mono-M2e-based and Tetra-M2e-based nanoassemblies in the form of monomer and tetramer, respectively (Fig. 11(b)). As the small size of antigen peptides limited their immunogenicity, the novel formed nanoassemblies allow them to be presented in high density in either monomeric or

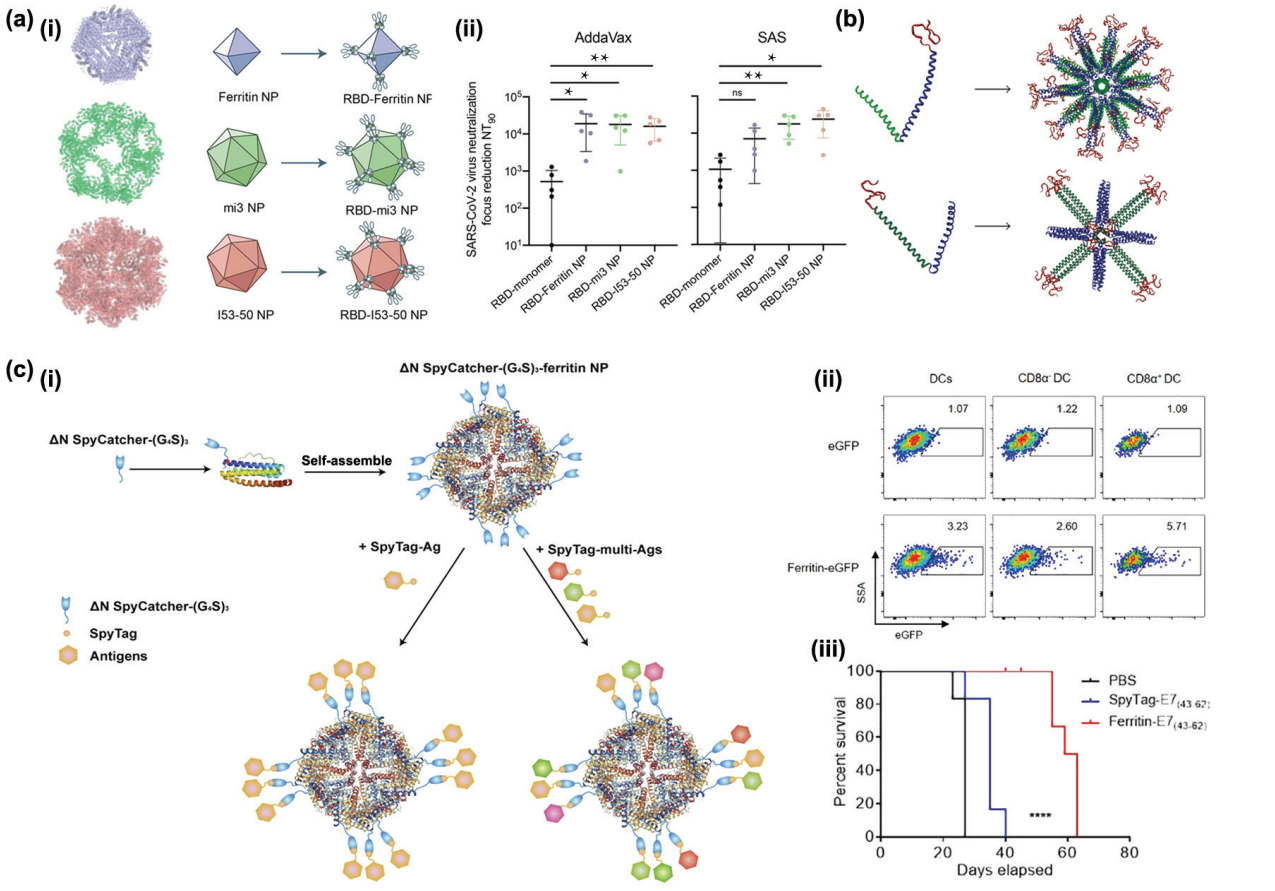

Figure 11 (a) Protein nanoassembly-based vaccines for the prevention of COVID-19. (i) Schematic design of three different RBD-conjugated nanoassemblies. (ii) SARS-CoV-2 live virus neutralization assay using different designed vaccines. Reproduced with permission from Ref. [208], © American Chemical Society 2021. (b) Computer model of Mono-M2e NPs (upper) and Tetra-M2e NPs (below) for AI immune therapy. Reproduced with permission from Ref. [212], © Babapoor, S. et al. 2011. (c) Fn nanoassembly-based vaccines for cancer immunotherapy. (i) Schematic design of the construction of Fn-based vaccines by SpyTag/SpyCatcher technology. (ii) Flow cytometry analysis of capture efficiency of DCs towards eGFP and ferritin-eGFP. (iii) The survival curve of TC-1-bearing mice receiving different treatments. Reproduced with permission from Ref. [215], © Elsevier Inc. 2018.

tetrameric formation. The diameter of Mono-M2e and Tetra-M2e were around 35 and 23 nm respectively. Compared with the unvaccinated group, the M2e specific IgG response of chickens vaccinated with Mono-M2e or Tetra-M2e was observed. When coupled with adjuvants, the vaccine Tetra-M2e elicited an extremely higher antibody response than Mono-M2e. Besides, the Tetra-M2e with adjuvants offered a dramatic improvement in protection, compared to Mono-M2e and PBS groups, against subtype H5N2 of low-pathogenicity AI virus by reduction of the AI virus shedding.

Kelly and coworkers employed MVP-based vault to load major outer membrane protein (MOMP) of *Chlamydia muridarum* for the preparation of MOMP-vault vaccine against mucosal infections [213]. Intranasal immunity with MOMP-vault activated anti-chlamydia response and significantly reduced bacterial burden. Besides, MOMP-vault coupled with adjuvants enhanced microbial eradication without inducing inflammation. The bacterial burden of chlamydiae following an infectious challenge was statistically reduced in the MOMP-vault immunized group compared to the only vault immunized group.

Cancer vaccine has become one of the most promising strategies for activating own immune system to eliminate tumors. Steinmetz and coworkers designed a tumor-specific vaccine PhMV-CH401 by using PhMV-based VLPs as the platform and human epidermal growth factor receptor-2 (HER2) derived CH401 peptide epitope as the antigen [214]. MTT assays showed that PhMV-CH401 enhanced cytotoxicity towards DDHER2 tumor cells than CH401 only. In addition, whether loaded with Toll-like receptor 9 (TLR9) agonists CpG adjuvant or not, PhMV-CH401 was able to elicit a strong immune response and produce high titers of HER2-specific immunoglobulins *in vivo*. The survival period of the vaccinated BALB/C mice bearing DDHER2 tumor was remarkably prolonged compared to the unvaccinated group.

Wang et al. utilized the SpyTag/SpyCather conjugation strategy for the modification of antigen on the Fn-based nanoassembly to set up a flexible and efficient vaccine platform for tumor therapy [215]. SpyCatcher was fused with ferritin, while SpyTag was fused with HPV16 oncogene E7 peptide antigen or eGFP (Fig. 11(c)). After simple mixing, an isopeptide bond can be formed between SpyTag and SpyCatcher to facilitate the modification of antigen or eGFP onto the Fn-based nanoassemblies. Compared to free eGFP, ferritin-eGFP nanoparticles were more efficiently uptaken by DCs, particularly by $CD8\alpha^+$ population. The formed ferritin-E7 nanoparticle could be more efficiently captured by draining lymph nodes than individual ligand E7. After being treated by ferritin-E7 nanoparticle with CpG, TC-1 bearing mice showed a longer survival time than the group receiving ligand E7 coupled with CpG.

Amidi and coworkers developed an anticancer vaccine nanoparticle based on a self-assemblable peptide (Ac-AAVVLLLW-COOH) to carry various antigens [216]. Peptide antigens, ovalbumin$(OVA)_{250-264}$ and HPV16 $E7_{43-57}$, were conjugated to the N-terminal of the self-assemblable peptide to generate fusion peptides OVA-SA and HPV-SA, respectively. When combined with CpG adjuvant, nanoparticles assembled from either OVA-SA or HPV-SA could induce an increment of

antigen-specific $CD8^+$ T cells in mice. On the TC-1-bearing mice, vaccination of HPV-SA coupled with CpG showed an increased survival period in contrast to the group of HPV peptide coupled with CpG, which indicated that the soluble peptide antigen even combined with a strong adjuvant is not effective, while the antigen in the form of a designated structure could be efficiently processed and presented by DCs for better immune response.

5 Clinical application and potential

In the aspect of vaccine development, a number of VLP-based vaccines have been approved for clinical use to prevent HPV (Cervarix®, Gardasil® and Gardasil 9®, Gene Vac-B®, Revac-B®, Shanvac-B®), hepatitis B (Engerix-B®), hepatitis E (Hecolin®), and COVID-19 (Covifenz®). In addition, increasing VLP-based vaccine candidates have entered preclinical and clinical trials for diseases including COVID-19 [197], seasonal Influenza [198], Malaria [199], and Influenza (H5N1, H1N1 virus) [200–202]. Fn-based nanoassembly as another promising vaccine platform have shown great market prospects with several candidates in clinical trials against different diseases, including influenza (ClinicalTrials.gov ID: NCT03186781), COVID-19 (ClinicalTrials.gov ID: NCT04784767), and Epstein-Barr virus (EBV) (ClinicalTrials.gov ID: NCT04784767).

In the aspect of drug delivery, although still few reports of clinical research have been reported, a growing body of investigations have shown that protein/peptide-based nanoassmblies have significant promise. Among them, Fn-based nanoassembly with excellent biocompatibility, low immunogenicity, intrinsic tumor targeting, and favorable pharmacokinetics have the greatest potential to enter the clinic. Six patents related to the construction and modification of Fn-based nanoassembly for the loading of various therapeutics in recent two years (Nos. US20200138960A1, US10640775B2, US20210403515A1, US20210363194A1, WO2021008454A1, and US20210393539A1) highlight the distinctive prospect of Fn-based nanoassembly for drug delivery.

6 Conclusion and outlook

Due to excellent biocompatibility and degradability, high-ordered architectures, and abundant modifiable interfaces and amino acid residues, assemblable proteins/peptides have shown great potential in the construction of nanoplatforms for biomedicine application. Heterologous expression is the most commonly-used strategy that can produce biomaterials with unified molecular weight in a green, gentle, and economical way. In addition, fusing therapeutic or functional protein/peptides into the backbone by genetic engineering allows for the precise customization of assemblable proteins/peptides.

Numerous studies indicated that the parameters of quantity, distribution, and orientation of targeting ligand can influence the targeting efficiency in drug delivery, which is related to the clustering of receptors on the surface of target cells, cellular endocytosis, and opsonin. For vaccine development, the parameters of size, geometry, and surface structure significantly affect immune response, which is attributed to the uptake of APCs, retention of lymph nodes, and antigen presentation. Taken together, precise customization of nanoassemblies is crucial for the construction of highly efficient drug carriers and vaccine platforms. Assemblable proteins/peptides with controllable self-assembling ability and precise modifiability endure the precise customization of nanoassemblies with defined morphology and modification.

Protein nanocages and VLPs as multimeric protein assemblies with specific and crucial physiological and pathological role, have the merits of superior functional control, higher-level complexity, and stability. Owing to the relatively simple sequence and spatial structure of nanostructures assembled from natural proteins and artificial peptides, the multifunctional and responsive assemblable proteins/peptides can be easily created by adopting flexible and unbounded combinable modularized structures.

However, various drawbacks still exist at this stage, such as lack of comprehensive and systematic understanding of the relationship between protein structure and function, difficulty in the accurate prediction for design and modification of the protein, and low efficiency of the expression system. With the rapid development and integration of modern biotechnology and computer science, combined with biological engineering such as genetic engineering and fermentation engineering, these bottlenecks will be continuously broken through.

Acknowledgements

This work was supported by the National Key Research and Development Program of China (No. 2019YFA0905200), the National Natural Science Foundation of China (No. 82072045), and the Natural Science Foundation of Jiangsu Province of China for Excellent Young Scholars (No. BK20190084).

References

[1] Hoonjan, M.; Sachdeva, G.; Chandra, S.; Kharkar, P. S.; Sahu, N.; Bhatt, P. Investigation of HSA as a biocompatible coating material for arsenic trioxide nanoparticles. *Nanoscale* **2018**, *10*, 8031–8041.

[2] Krauss, I. R.; Picariello, A.; Vitiello, G.; De Santis, A.; Koutsioubas, A.; Houston, J. E.; Fragneto, G.; Paduano, L. Interaction with human serum proteins reveals biocompatibility of phosphocholine-functionalized spions and formation of albumin-decorated nanoparticles. *Langmuir* **2020**, *36*, 8777–8791.

[3] Wang, L. R.; Lin, H. Y.; Chi, X. Q.; Sun, C. J.; Huang, J. Q.; Tang, X. X.; Chen, H. M.; Luo, X. J.; Yin, Z. Y.; Gao, J. H. A self-assembled biocompatible nanoplatform for multimodal MR/fluorescence imaging assisted photothermal therapy and prognosis analysis. *Small* **2018**, *14*, 1801612.

[4] Pan, G. H.; Ni, J.; Wei, Y. F.; Yu, G. L.; Gentz, R.; Dixit, V. M. An antagonist decoy receptor and a death domain-containing receptor for TRAIL. *Science* **1997**, *277*, 815–818.

[5] Tan, C. Y.; Ban, H.; Kim, Y. H.; Lee, S. K. The heat shock protein 27 (Hsp27) operates predominantly by blocking the mitochondrial-independent/extrinsic pathway of cellular apoptosis. *Mol. Cells* **2009**, *27*, 703.

[6] Li, J. Y.; Paragas, N.; Ned, R. M.; Qiu, A. D.; Viltard, M.; Leete, T.; Drexler, I. R.; Chen, X.; Sanna-Cherchi, S.; Mohammed, F. et al. Scara5 is a ferritin receptor mediating non-transferrin iron delivery. *Dev. Cell* **2009**, *16*, 35–46.

[7] Liu, J. L.; Chen, B. X.; Zhao, B.; Luo, X. B.; Li, J. F.; Xie, Y. T.; Li, B. L.; Chen, H. Y.; Zhao, M. Y.; Yan, H. D. Effect of hirudin on arterialized venous flap survival in rabbits. *Biomed. Pharmacother.* **2021**, *142*, 111981.

[8] Ki, M. R.; Kim, J. K.; Kim, S. H.; Nguyen, T. K. M.; Kim, K. H.; Pack, S. P. Compartment-restricted and rate-controlled dual drug delivery system using a biosilica-enveloped ferritin cage. *J. Ind. Eng. Chem.* **2020**, *81*, 367–374.

[9] Murata, M.; Narahara, S.; Kawano, T.; Hamano, N.; Piao, J. S.; Kang, J. H.; Ohuchida, K.; Murakami, T.; Hashizume, M. Design and function of engineered protein nanocages as a drug delivery system for targeting pancreatic cancer cells via neuropilin-1. *Mol. Pharm.* **2015**, *12*, 1422–1430.

[10] Reuter, L. J.; Shahbazi, M. A.; Mäkilä, E. M.; Salonen, J. J.; Saberianfar, R.; Menassa, R.; Santos, H. A.; Joensuu, J. J.; Ritala, A. Coating nanoparticles with plant-produced transferrin-hydrophobin fusion protein enhances their uptake in cancer cells. *Bioconjug. Chem.* **2017**, *28*, 1639–1648.

[11] Lucon, J.; Abedin, M. J.; Uchida, M.; Liepold, L.; Jolley, C. C.;

Young, M.; Douglas, T. A click chemistry based coordination polymer inside small heat shock protein. *Chem. Commun.* **2010**, *46*, 264–266.
[12] Varpness, Z.; Suci, P. A.; Ensign, D.; Young, M. J.; Douglas, T. Photosensitizer efficiency in genetically modified protein cage architectures. *Chem. Commun.* **2009**, 3726–3728.
[13] Gillitzer, E.; Willits, D.; Young, M.; Douglas, T. Chemical modification of a viral cage for multivalent presentation. *Chem. Commun.* **2002**, 2390–2391.
[14] Ding, D.; Yang, C.; Lv, C.; Li, J.; Tan, W. H. Improving tumor accumulation of aptamers by prolonged blood circulation. *Anal. Chem.* **2020**, *92*, 4108–4114.
[15] Brandt, M.; Cardinale, J.; Giammei, C.; Guarrochena, X.; Happl, B.; Jouini, N.; Mindt, T. L. Mini-review: Targeted radiopharmaceuticals incorporating reversible, low molecular weight albumin binders. *Nucl. Med. Biol.* **2019**, *70*, 46–52.
[16] Chen, X.; Ling, X.; Zhao, L. L.; Xiong, F.; Hollett, G.; Kang, Y.; Barrett, A.; Wu, J. Biomimetic shells endow sub-50 nm nanoparticles with ultrahigh paclitaxel payloads for specific and robust chemotherapy. *ACS. Appl. Mater. Interfaces* **2018**, *10*, 33976–33985.
[17] Wang, M. Y.; Zhang, L.; Cai, Y. F.; Yang, Y.; Qiu, L. P.; Shen, Y. T.; Jin, J.; Zhou, J.; Chen, J. H. Bioengineered human serum albumin fusion protein as target/enzyme/pH three-stage propulsive drug vehicle for tumor therapy. *ACS Nano* **2020**, *14*, 17405–17418.
[18] Desai, N.; Trieu, V.; Yao, Z. W.; Louie, L.; Ci, S.; Yang, A.; Tao, C. L.; De, T.; Beals, B.; Dykes, D. et al. Increased antitumor activity, intratumor paclitaxel concentrations, and endothelial cell transport of cremophor-free, albumin-bound paclitaxel, ABI-007, compared with cremophor-based paclitaxel. *Clin. Cancer Res.* **2006**, *12*, 1317–1324.
[19] Wang, D. F.; Liang, N.; Kawashima, Y.; Cui, F. D.; Yan, P. F.; Sun, S. P. Biotin-modified bovine serum albumin nanoparticles as a potential drug delivery system for paclitaxel. *J. Mater. Sci.* **2019**, *54*, 8613–8626.
[20] Das, R. P.; Singh, B. G.; Kunwar, A.; Ramani, M. V.; Subbaraju, G. V.; Hassan, P. A.; Priyadarsini, K. I. Tuning the binding, release and cytotoxicity of hydrophobic drug by bovine serum albumin nanoparticles: Influence of particle size. *Colloids Surf. B Biointerfaces* **2017**, *158*, 682–688.
[21] Gong, T.; Tan, T. T.; Zhang, P.; Li, H. H.; Deng, C. F.; Huang, Y.; Gong, T.; Zhang, Z. R. Palmitic acid-modified bovine serum albumin nanoparticles target scavenger receptor-A on activated macrophages to treat rheumatoid arthritis. *Biomaterials* **2020**, *258*, 120296.
[22] Nosrati, H.; Abbasi, R.; Charmi, J.; Rakhshbahar, A.; Aliakbarzadeh, F.; Danafar, H.; Davaran, S. Folic acid conjugated bovine serum albumin: An efficient smart and tumor targeted biomacromolecule for inhibition folate receptor positive cancer cells. *Int. J. Biol. Macromol.* **2018**, *117*, 1125–1132.
[23] Gaowa, A.; Horibe, T.; Kohno, M.; Sato, K.; Harada, H.; Hiraoka, M.; Tabata, Y.; Kawakami, K. Combination of hybrid peptide with biodegradable gelatin hydrogel for controlled release and enhancement of anti-tumor activity *in vivo*. *J. Controlled Release* **2014**, *176*, 1–7.
[24] Chen, X. J.; Zou, J. F.; Zhang, K.; Zhu, J. J.; Zhang, Y.; Zhu, Z. H.; Zheng, H. Y.; Li, F. Z.; Piao, J. G. Photothermal/matrix metalloproteinase-2 dual-responsive gelatin nanoparticles for breast cancer treatment. *Acta. Pharm. Sin. B* **2021**, *11*, 271–282.
[25] Zhou, H.; He, G.; Sun, Y. B.; Wang, J. G.; Wu, H. T.; Jin, P.; Zha, Z. Cryptobiosis-inspired assembly of "AND" logic gate platform for potential tumor-specific drug delivery. *Acta Pharm. Sin. B* **2021**, *11*, 534–543.
[26] He, G.; Chen, S.; Xu, Y. J.; Miao, Z. H.; Ma, Y.; Qian, H. S.; Lu, Y.; Zha, Z. B. Charge reversal induced colloidal hydrogel acts as a multi-stimuli responsive drug delivery platform for synergistic cancer therapy. *Mater. Horiz.* **2019**, *6*, 711–716.
[27] Cheng, W. Y.; Wang, B. L.; Zhang, C. Y.; Dong, Q. N.; Qian, J. J.; Zha, L.; Chen, W. D.; Hong, L. F. Preparation and preliminary pharmacokinetics study of GNA-loaded zein nanoparticles. *J. Pharm. Pharmacol.* **2019**, *71*, 1626–1634.
[28] Bao, X. Y.; Qian, K.; Yao, P. Oral delivery of exenatide-loaded hybrid zein nanoparticles for stable blood glucose control and β-cell repair of type 2 diabetes mice. *J. Nanobiotechnol.* **2020**, *18*, 67.
[29] Shinde, P.; Agraval, H.; Singh, A.; Yadav, U. C. S.; Kumar, U. Synthesis of luteolin loaded zein nanoparticles for targeted cancer therapy improving bioavailability and efficacy. *J. Drug. Deliv. Sci. Technol.* **2019**, *52*, 369–378.
[30] Alqahtani, M. S.; Syed, R.; Alshehri, M. Size-dependent phagocytic uptake and immunogenicity of gliadin nanoparticles. *Polymers* **2020**, *12*, 2576.
[31] Yang, Y. Y.; Zhang, M.; Liu, Z. P.; Wang, K.; Yu, D. G. Meletin sustained-release gliadin nanoparticles prepared via solvent surface modification on blending electrospraying. *Appl. Surf. Sci.* **2018**, *434*, 1040–1047.
[32] Qian, X. P.; Ge, L.; Yuan, K. J.; Li, C.; Zhen, X.; Cai, W. B.; Cheng, R. S.; Jiang, X. Q. Targeting and microenvironment-improving of phenylboronic acid-decorated soy protein nanoparticles with different sizes to tumor. *Theranostics* **2019**, *9*, 7417–7430.
[33] Farooq, M. A.; Aquib, M.; Ghayas, S.; Bushra, R.; Haleem Khan, D.; Parveen, A.; Wang, B. Whey protein: A functional and promising material for drug delivery systems recent developments and future prospects. *Polym. Adv. Technol.* **2019**, *30*, 2183–2191.
[34] Castro, M. A. A.; Alric, I.; Brouillet, F.; Peydecastaing, J.; Fullana, S. G.; Durrieu, V. Spray-dried succinylated soy protein microparticles for oral ibuprofen delivery. *AAPS PharmSciTech* **2019**, *20*, 79.
[35] Tang, J. H.; Zhou, J. P.; Chen, F. H.; Sun, T. T.; Kuang, W. J.; Feng, R. X. Synthesis, characterization and drug-loading capacity of novel amphiphilic amino acid copolymer. *J. China Pharm. Univ.* **2012**, *43*, 211–215.
[36] Loureiro, A.; Nogueira, E.; Azoia, N. G.; Sária, M. P.; Abreu, A. S.; Shimanovich, U.; Rollett, A.; Härmark, J.; Hebert, H.; Guebitz, G. et al. Size controlled protein nanoemulsions for active targeting of folate receptor positive cells. *Colloids Surf. B Biointerfaces* **2015**, *135*, 90–98.
[37] Yang, P. P.; Zhang, K.; He, P. P.; Fan, Y.; Gao X. J.; Gao, X. F.; Chen, Z. M.; Hou, D. Y.; Li, Y.; Yi, Y. et al. A biomimetic platelet based on assembling peptides initiates artificial coagulation. *Sci. Adv.* **2020**, *6*, eaaz4107.
[38] Bao, C. Y.; Yin, Y. H.; Zhang, Q. Synthesis and assembly of laccase-polymer giant amphiphiles by self-catalyzed CuAAC click chemistry. *Biomacromolecules* **2018**, *19*, 1539–1551.
[39] Mohammad-Beigi, H.; Shojaosadati, S. A.; Morshedi, D.; Arpanaei, A.; Marvian, A. T. Preparation and *in vitro* characterization of gallic acid-loaded human serum albumin nanoparticles. *J. Nanopart. Res.* **2015**, *17*, 167.
[40] Li, W.; Garringer, H. J.; Goodwin, C. B.; Richine, B.; Acton, A.; VanDuyn, N.; Muhoberac, B. B.; Irimia-Dominguez, J.; Chan, R. J.; Peacock, M. et al. Systemic and cerebral iron homeostasis in ferritin knock-out mice. *PLoS One* **2015**, *10*, e0117435.
[41] Thompson, K.; Menzies, S.; Muckenthaler, M.; Torti, F. M.; Wood, T.; Torti, S. V.; Hentze, M. W.; Beard, J.; Connor, J. Mouse brains deficient in H-ferritin have normal iron concentration but a protein profile of iron deficiency and increased evidence of oxidative stress. *J. Neurosci. Res.* **2003**, *71*, 46–63.
[42] Pieters, B. J. G. E.; Van Eldijk, M. B.; Nolte, R. J. M.; Mecinović, J. Natural supramolecular protein assemblies. *Chem. Soc. Rev.* **2016**, *45*, 24–39.
[43] Carmona, F.; Poli, M.; Bertuzzi, M.; Gianoncelli, A.; Gangemi, F.; Arosio, P. Study of ferritin self-assembly and heteropolymer formation by the use of fluorescence resonance energy transfer (FRET) technology. *Biochim. Biophys. Acta. Gen. Subj.* **2017**, *1861*, 522–532.
[44] Wege, C.; Koch, C. From stars to stripes: RNA-directed shaping of plant viral protein templates-structural synthetic virology for smart biohybrid nanostructures. *Wiley Interdiscip. Rev. Nanomed. Nanobiotechnol.* **2020**, *12*, e1591.
[45] Fiedler, J. D.; Fishman, M. R.; Brown, S. D.; Lau, J.; Finn, M. G.

Multifunctional enzyme packaging and catalysis in the Qβ protein nanoparticle. *Biomacromolecules* **2018**, *19*, 3945–3957.
[46] Wang, J. C.; Liu, Y. C.; Chen, Y. M.; Zhang, T.; Wang, A. P.; Wei, Q.; Liu, D. M.; Wang, F. Y.; Zhang, G. P. Capsid assembly is regulated by amino acid residues asparagine 47 and 48 in the VP2 protein of porcine parvovirus. *Vet. Microbiol.* **2021**, *253*, 108974.
[47] Harrison, P. M.; Arosio, P. The ferritins: Molecular properties, iron storage function and cellular regulation. *Biochim. Biophys. Acta Bioenerg.* **1996**, *1275*, 161–203.
[48] Arosio, P.; Elia, L.; Poli, M. Ferritin, cellular iron storage and regulation. *IUBMB Life* **2017**, *69*, 414–422.
[49] Uchida, M.; Kang, S.; Reichhardt, C.; Harlen, K.; Douglas, T. The ferritin superfamily: Supramolecular templates for materials synthesis. *Biochim. Biophys. Acta. Gen. Subj.* **2010**, *1800*, 834–845.
[50] Harrison, P. M.; Fischbach, F. A.; Hoy, T. G.; Haggis, G. H. Ferric oxyhydroxide core of ferritin. *Nature* **1967**, *216*, 1188–1190.
[51] Bertini, I.; Lalli, D.; Mangani, S.; Pozzi, C.; Rosa, C.; Theil, E. C.; Turano, P. Structural insights into the ferroxidase site of ferritins from higher eukaryotes. *J. Am. Chem. Soc.* **2012**, *134*, 6169–6176.
[52] Arosio, P.; Ingrassia, R.; Cavadini, P. Ferritins: A family of molecules for iron storage, antioxidation and more. *Biochim. Biophys. Acta. Gen. Subj.* **2009**, *1790*, 589–599.
[53] Torti, F. M.; Torti, S. V. Regulation of ferritin genes and protein. *Blood* **2002**, *99*, 3505–3516.
[54] Damiani, V.; Falvo, E.; Fracasso, G.; Federici, L.; Pitea, M.; De Laurenzi, V.; Sala, G.; Ceci, P. Therapeutic efficacy of the novel stimuli-sensitive nano-ferritins containing doxorubicin in a head and neck cancer model. *Int. J. Mol. Sci.* **2017**, *18*, 1555.
[55] Fracasso, G.; Falvo, E.; Colotti, G.; Fazi, F.; Ingegnere, T.; Amalfitano, A.; Doglietto, G. B.; Alfieri, S.; Boffi, A.; Morea, V. et al. Selective delivery of doxorubicin by novel stimuli-sensitive nano-ferritins overcomes tumor refractoriness. *J. Controlled Release* **2016**, *239*, 10–18.
[56] Falvo, E.; Tremante, E.; Arcovito, A.; Papi, M.; Elad, N.; Boffi, A.; Morea, V.; Conti, G.; Toffoli, G.; Fracasso, G. et al. Improved doxorubicin encapsulation and pharmacokinetics of ferritin-fusion protein nanocarriers bearing proline, serine, and alanine elements. *Biomacromolecules* **2016**, *17*, 514–522.
[57] Huang, C.; Chu, C. C.; Wang, X. Y.; Lin, H. R.; Wang, J. Q.; Zeng, Y.; Zhu, W. Z.; Wang, Y. X. J.; Liu, G. Ultra-high loading of sinoporphyrin sodium in ferritin for single-wave motivated photothermal and photodynamic co-therapy. *Biomater. Sci.* **2017**, *5*, 1512–1516.
[58] Pandolfi, L.; Bellini, M.; Vanna, R.; Morasso, C.; Zago, A.; Carcano, S.; Avvakumova, S.; Bertolini, J. A.; Rizzuto, M. A.; Colombo, M. et al. H-ferritin enriches the curcumin uptake and improves the therapeutic efficacy in triple negative breast cancer cells. *Biomacromolecules* **2017**, *18*, 3318–3330.
[59] Falvo, E.; Malagrinò, F.; Arcovito, A.; Fazi, F.; Colotti, G.; Tremante, E.; Di Micco, P.; Braca, A.; Opri, R.; Giuffrè, A. et al. The presence of glutamate residues on the PAS sequence of the stimuli-sensitive nano-ferritin improves *in vivo* biodistribution and mitoxantrone encapsulation homogeneity. *J. Controlled Release* **2018**, *275*, 177–185.
[60] Ryser, H.; Caulfield, J. B.; Aub, J. C. Studies on protein uptake by isolated tumor cells. I. Electron microscopic evidence of ferritin uptake by ehrlich ascites tumor cells. *J. Cell Biol.* **1962**, *14*, 255–268.
[61] Caulfield, J. B. Studies on ferritin uptake by isolated tumor cells. *Lab. Invest.* **1963**, *12*, 1018–1025.
[62] Easty, G. C.; Yarnell, M. M.; Andrews, R. D. The uptake of proteins by normal and tumour cells *in vitro*. *Br. J. Cancer* **1965**, *18*, 354–367.
[63] Li, L.; Fang, C. J.; Ryan, J. C.; Niemi, E. C.; Lebrón, J. A.; Björkman, P. J.; Arase, H.; Torti, F. M.; Torti, S. V.; Nakamura, M. C. et al. Binding and uptake of H-ferritin are mediated by human transferrin receptor-1. *Proc. Natl. Acad. Sci. USA* **2010**, *107*, 3505–3510.
[64] Kawabata, H. Transferrin and transferrin receptors update. *Free Radic. Biol. Med.* **2019**, *133*, 46–54.
[65] Fan, K. L.; Cao, C. Q.; Pan, Y. X.; Lu, D.; Yang, D. L.; Feng, J.; Song, L. N.; Liang, M. M.; Yan, X. Y. Magnetoferritin nanoparticles for targeting and visualizing tumour tissues. *Nat. Nanotechnol.* **2012**, *7*, 765.
[66] Wang, B.; Tang, M.; Yuan, Z.; Li, Z.; Hu, B.; Bai, X.; Chu, J.; Xu, X.; Zhang, X. Targeted delivery of a sting agonist to brain tumors using bioengineered protein nanoparticles for enhanced immunotherapy. *Bioact. Mater.* **2022**, *16*, 232–248.
[67] Lajoie, J. M.; Shusta, E. V. Targeting receptor-mediated transport for delivery of biologics across the blood-brain barrier. *Annu. Rev. Pharmacol. Toxicol.* **2015**, *55*, 613–631.
[68] Fan, K. L.; Jia, X. H.; Zhou, M.; Wang, K.; Conde, J.; He, J. Y.; Tian, J.; Yan, X. Y. Ferritin nanocarrier traverses the blood brain barrier and kills glioma. *ACS Nano* **2018**, *12*, 4105–4115.
[69] Richter, K.; Haslbeck, M.; Buchner, J. The heat shock response: Life on the verge of death. *Mol. Cell.* **2010**, *40*, 253–266.
[70] Guo, M.; Liu, J. H.; Ma, X.; Luo, D. X.; Gong, Z. H.; Lu, M. H. The plant heat stress transcription factors (HSFs): Structure, regulation, and function in response to abiotic stresses. *Front. Plant Sci.* **2016**, *7*, 114.
[71] Shende, P.; Bhandarkar, S.; Prabhakar, B. Heat shock proteins and their protective roles in stem cell biology. *Stem Cell Rev. Rep.* **2019**, *15*, 637–651.
[72] Smith, D. F.; Whitesell, L.; Katsanis, E. Molecular chaperones: Biology and prospects for pharmacological intervention. *Pharmacol. Rev.* **1998**, *50*, 493–514.
[73] Tsukahara, F.; Yoshioka, T.; Muraki, T. Molecular and functional characterization of HSC54, a novel variant of human heat-shock cognate protein 70. *Mol. Pharmacol.* **2000**, *58*, 1257–1263.
[74] Stromer, T.; Fischer, E.; Richter, K.; Haslbeck, M.; Buchner, J. Analysis of the regulation of the molecular chaperone Hsp26 by temperature-induced dissociation: The N-terminal domain is important for oligomer assembly and the binding of unfolding proteins. *J. Biol. Chem.* **2004**, *279*, 11222–11228.
[75] Kim, K. K.; Kim, R.; Kim, S. H. Crystal structure of a small heat-shock protein. *Nature* **1998**, *394*, 595–599.
[76] Kim, R.; Kim, K. K.; Yokota, H.; Kim, S. H. Small heat shock protein of *Methanococcus jannaschii*, a hyperthermophile. *Proc. Natl. Acad. Sci. USA* **1998**, *95*, 9129–9133.
[77] Kim, K. K.; Yokota, H.; Santoso, S.; Lerner, D.; Kim, R.; Kim, S. H. Purification, crystallization, and preliminary X-ray crystallographic data analysis of small heat shock protein homolog from *Methanococcus jannaschii*, a hyperthermophile. *J. Struct. Biol.* **1998**, *121*, 76–80.
[78] Flenniken, M. L.; Willits, D. A.; Brumfield, S.; Young, M. J.; Douglas, T. The small heat shock protein cage from *Methanococcus jannaschii* is a versatile nanoscale platform for genetic and chemical modification. *Nano Lett.* **2003**, *3*, 1573–1576.
[79] Bova, M. P.; Ding, L. L.; Horwitz, J.; Fung, B. K. K. Subunit exchange of αA-crystallin. *J. Biol. Chem.* **1997**, *272*, 29511–29517.
[80] Choi, S. H.; Kwon, I. C.; Hwang, K. Y.; Kim, I. S.; Ahn, H. J. Small heat shock protein as a multifunctional scaffold: Integrated tumor targeting and caspase imaging within a single cage. *Biomacromolecules* **2011**, *12*, 3099–3106.
[81] Flenniken, M. L.; Liepold, L. O.; Crowley, B. E.; Willits, D. A.; Young, M. J.; Douglas, T. Selective attachment and release of a chemotherapeutic agent from the interior of a protein cage architecture. *Chem. Commun.* **2005**, 447–449.
[82] Kawano, T.; Murata, M.; Kang, J. H.; Piao, J. S.; Narahara, S.; Hyodo, F.; Hamano, N.; Guo, J.; Oguri, S.; Ohuchida, K. et al. Ultrasensitive MRI detection of spontaneous pancreatic tumors with nanocage-based targeted contrast agent. *Biomaterials* **2018**, *152*, 37–46.
[83] Suprenant, K. A. Vault ribonucleoprotein particles: Sarcophagi, gondolas, or safety deposit boxes. *Biochemistry* **2002**, *41*, 14447–14454.
[84] Van Zon, A.; Mossink, M. H.; Scheper, R. J.; Sonneveld, P.; Wiemer, E. A. C. The vault complex. *Cell. Mol. Life Sci.* **2003**, *60*, 1828–1837.
[85] Kedersha, N. L.; Rome, L. H. Isolation and characterization of a novel ribonucleoprotein particle: Large structures contain a single

species of small RNA. *J. Cell Biol.* **1986**, *103*, 699–709.
[86] Ding, K.; Zhang, X.; Mrazek, J.; Kickhoefer, V. A.; Lai, M.; Ng, H. L.; Yang, O. O.; Rome, L. H.; Zhou, Z. H. Solution structures of engineered vault particles. *Structure* **2018**, *26*, 619–626.e3.
[87] Stephen, A. G.; Raval-Fernandes, S.; Huynh, T.; Torres, M.; Kickhoefer, V. A.; Rome, L. H. Assembly of vault-like particles in insect cells expressing only the major vault protein. *J. Biol. Chem.* **2001**, *276*, 23217–23220.
[88] Mikyas, Y.; Makabi, M.; Raval-Fernandes, S.; Harrington, L.; Kickhoefer, V. A.; Rome, L. H.; Stewart, P. L. Cryoelectron microscopy imaging of recombinant and tissue derived vaults: Localization of the MVP N termini and VPARP. *J. Mol. Biol.* **2004**, *344*, 91–105.
[89] Kickhoefer, V. A.; Liu, Y. E.; Kong, L. B.; Snow, B. E.; Stewart, P. L.; Harrington, L.; Rome, L. H. The telomerase/vault-associated protein TEP1 is required for vault RNA stability and its association with the vault particle. *J. Cell Biol.* **2001**, *152*, 157–164.
[90] Frascotti, G.; Galbiati, E.; Mazzucchelli, M.; Pozzi, M.; Salvioni, L.; Vertemara, J.; Tortora, P. The vault nanoparticle: A gigantic ribonucleoprotein assembly involved in diverse physiological and pathological phenomena and an ideal nanovector for drug delivery and therapy. *Cancers* **2021**, *13*, 707.
[91] Voth, B. L.; Pelargos, P. E.; Barnette, N. E.; Bhatt, N. S.; Chen, C. H. J.; Lagman, C.; Chung, L. K.; Nguyen, T.; Sheppard, J. P.; Romiyo, P. et al. Intratumor injection of CCL21-coupled vault nanoparticles is associated with reduction in tumor volume in an *in vivo* model of glioma. *J. Neurooncol.* **2020**, *147*, 599–605.
[92] Goldsmith, L. E.; Yu, M.; Rome, L. H.; Monbouquette, H. G. Vault nanocapsule dissociation into halves triggered at low pH. *Biochemistry* **2007**, *46*, 2865–2875.
[93] Esfandiary, R.; Kickhoefer, V. A.; Rome, L. H.; Joshi, S. B.; Middaugh, C. R. Structural stability of vault particles. *J. Pharm. Sci.* **2009**, *98*, 1376–1386.
[94] Barth, H.; Ulsenheimer, A.; Pape, G. R.; Diepolder, H. M.; Hoffmann, M.; Neumann-Haefelin, C.; Thimme, R.; Henneke, P.; Klein, R.; Paranhos-Baccala, G. et al. Uptake and presentation of hepatitis C virus-like particles by human dendritic cells. *Blood* **2005**, *105*, 3605–3614.
[95] Crisci, E.; Bárcena, J.; Montoya, M. Virus-like particles: The new frontier of vaccines for animal viral infections. *Vet. Immunol. Immunopathol.* **2012**, *148*, 211–225.
[96] Lin, T. W.; Chen, Z. G.; Usha, R.; Stauffacher, C. V.; Dai, J. B.; Schmidt, T.; Johnson, J. E. The refined crystal structure of cowpea mosaic virus at 2. 8 Å resolution. *Virology* **1999**, *265*, 20–34.
[97] Speir, J. A.; Bothner, B.; Qu, C. X.; Willits, D. A.; Young, M. J.; Johnson, J. E. Enhanced local symmetry interactions globally stabilize a mutant virus capsid that maintains infectivity and capsid dynamics. *J. Virol.* **2006**, *80*, 3582–3591.
[98] Cui, Z. C.; Gorzelnik, K. V.; Chang, J. Y.; Langlais, C.; Jakana, J.; Young, R.; Zhang, J. J. Structures of Qβ virions, virus-like particles, and the Qβ-murA complex reveal internal coat proteins and the mechanism of host lysis. *Proc. Natl. Acad. Sci. USA* **2017**, *114*, 11697–11702.
[99] Franzen, S.; Lommel, S. A. Targeting cancer with 'smart bombs': Equipping plant virus nanoparticles for a ' seek and destroy' mission. *Nanomedicine* **2009**, *4*, 575–588.
[100] Ren, Y. P.; Wong, S. M.; Lim, L. Y. Application of plant viruses as nano drug delivery systems. *Pharm. Res.* **2010**, *27*, 2509–2513.
[101] Chung, Y. H.; Cai, H.; Steinmetz, N. F. Viral nanoparticles for drug delivery, imaging, immunotherapy, and theranostic applications. *Adv. Drug Deliv. Rev.* **2020**, *156*, 214–235.
[102] Liu, J. L.; Dixit, A. B.; Robertson, K. L.; Qiao, E.; Black, L. W. Viral nanoparticle-encapsidated enzyme and restructured DNA for cell delivery and gene expression. *Proc. Natl. Acad. Sci. USA* **2014**, *111*, 13319–13324.
[103] Lam, P.; Steinmetz, N. F. Delivery of siRNA therapeutics using cowpea chlorotic mottle virus-like particles. *Biomater. Sci.* **2019**, *7*, 3138–3142.
[104] Frietze, K. M.; Peabody, D. S.; Chackerian, B. Engineering virus-like particles as vaccine platforms. *Curr. Opin. Virol.* **2016**, *18*, 44–49.
[105] Balke, I.; Zeltins, A. Use of plant viruses and virus-like particles for the creation of novel vaccines. *Adv. Drug Deliv. Rev.* **2019**, *145*, 119–129.
[106] Neek, M.; Kim, T. I.; Wang, S. W. Protein-based nanoparticles in cancer vaccine development. *Nanomed. Nanotechnol. Biol. Med.* **2019**, *15*, 164–174.
[107] Zepeda-Cervantes, J.; Ramírez-Jarquín, J. O.; Vaca, L. Interaction between virus-like particles (VLPs) and pattern recognition receptors (PRRs) from dendritic cells (DCs): Toward better engineering of VLPs. *Front. Immunol.* **2020**, *11*, 1100.
[108] Shukla, S.; Wang, C.; Beiss, V.; Cai, H.; Washington II, T.; Murray, A. A.; Gong, X. J.; Zhao, Z. C.; Masarapu, H.; Zlotnick, A. et al. The unique potency of cowpea mosaic virus (CPMV) *in situ* cancer vaccine. *Biomater. Sci.* **2020**, *8*, 5489–5503.
[109] Linder, M. B.; Szilvay, G. R.; Nakari-Setälä, T.; Penttilä, M. E. Hydrophobins: The protein-amphiphiles of filamentous fungi. *FEMS Microbiol. Rev.* **2005**, *29*, 877–896.
[110] Wessels, J. G. H. Hydrophobins: Proteins that change the nature of the fungal surface. *Adv. Microb. Physiol.* **1996**, *38*, 1–45.
[111] Wösten, H. A. B.; Scholtmeijer, K. Applications of hydrophobins: Current state and perspectives. *Appl. Microbiol. Biotechnol.* **2015**, *99*, 1587–1597.
[112] Wessels, J. G. H. Developmental regulation of fungal cell wall formation. *Annu. Rev. Phytopathol.* **1994**, *32*, 413–437.
[113] Kwan, A. H.; Winefield, R. D.; Sunde, M.; Matthews, J. M.; Haverkamp, R. G.; Templeton, M. D.; Mackay, J. P. Structural basis for rodlet assembly in fungal hydrophobins. *Proc. Natl. Acad. Sci. U.S.A.* **2006**, *103*, 3621–3626.
[114] Kallio, J. M.; Linder, M. B.; Rouvinen, J. Crystal structures of hydrophobin HFBII in the presence of detergent implicate the formation of fibrils and monolayer films. *J. Biol. Chem.* **2007**, *282*, 28733–28739.
[115] Fang, G. H.; Tang, B.; Liu, Z. T.; Gou, J. X.; Zhang, Y.; Xu, H.; Tang, X. Novel hydrophobin-coated docetaxel nanoparticles for intravenous delivery: *In vitro* characteristics and *in vivo* performance. *Eur. J. Pharm. Sci.* **2014**, *60*, 1–9.
[116] Maiolo, D.; Pigliacelli, C.; Moreno, P. S.; Violatto, M. B.; Talamini, L.; Tirotta, I.; Piccirillo, R.; Zucchetti, M.; Morosi, L.; Frapolli, R. et al. Bioreducible hydrophobin-stabilized supraparticles for selective intracellular release. *ACS Nano* **2017**, *11*, 9413–9423.
[117] Holt, C.; Carver, J. A.; Ecroyd, H.; Thorn, D. C. *Invited review*: Caseins and the casein micelle: Their biological functions, structures, and behavior in foods. *J. Dairy Sci.* **2013**, *96*, 6127–6146.
[118] Artym, J.; Zimecki, M. Milk-derived proteins and peptides in clinical trials. *Postepy Hig. Med. Dosw.* **2013**, *67*, 800–816.
[119] Elzoghby, A. O.; Abo El-Fotoh, W. S.; Elgindy, N. A. Casein-based formulations as promising controlled release drug delivery systems. *J. Controlled Release* **2011**, *153*, 206–216.
[120] Horne, D. S. Casein structure, self-assembly and gelation. *Curr. Opin. Colloid Interface Sci.* **2002**, *7*, 456–461.
[121] Huppertz, T.; De Kruif, C. G. Structure and stability of nanogel particles prepared by internal cross-linking of casein micelles. *Int. Dairy J.* **2008**, *18*, 556–565.
[122] Kumosinski, T. F.; Brown, E. M.; Farrell, H. M. Jr. Three-dimensional molecular modeling of bovine caseins: An energy-minimized *β*-casein structure. *J. Dairy Sci.* **1993**, *76*, 931–945.
[123] Tai, M. S.; Kegeles, G. A micelle model for the sedimentation behavior of bovine β-casein. *Biophys. Chem.* **1984**, *20*, 81–87.
[124] Portnaya, I.; Ben-Shoshan, E.; Cogan, U.; Khalfin, R.; Fass, D.; Ramon, O.; Danino, D. Self-assembly of bovine β-casein below the isoelectric pH. *J. Agric. Food Chem.* **2008**, *56*, 2192–2198.
[125] Javor, G. T.; Sood, S. M.; Chang, P.; Slattery, C. W. Interactions of triply phosphorylated human β-casein: Fluorescence spectroscopy and light-scattering studies of conformation and self-association. *Arch. Biochem. Biophys.* **1991**, *289*, 39–46.
[126] Livney, Y. D. Milk proteins as vehicles for bioactives. *Curr. Opin. Colloid Interface Sci.* **2010**, *15*, 73–83.

[127] Trejo, R.; Dokland, T.; Jurat-Fuentes, J.; Harte, F. Cryo-transmission electron tomography of native casein micelles from bovine milk. *J. Dairy Sci.* **2011**, *94*, 5770–5775.
[128] Pasquali-Ronchetti, I.; Baccarani-Contri, M. Elastic fiber during development and aging. *Microsc. Res. Tech.* **1997**, *38*, 428–435.
[129] Martyn, C.; Greenwald, S. A hypothesis about a mechanism for the programming of blood pressure and vascular disease in early life. *Clin. Exp. Pharmacol. Physiol.* **2001**, *28*, 948–951.
[130] Faury, G. Function–structure relationship of elastic arteries in evolution: From microfibrils to elastin and elastic fibres. *Pathol. Biol.* **2001**, *49*, 310–325.
[131] Tatham, A. S.; Shewry, P. R. Elastomeric proteins: Biological roles, structures and mechanisms. *Trends Biochem. Sci.* **2000**, *25*, 567–571.
[132] Yeboah, A.; Cohen, R. I.; Rabolli, C.; Yarmush, M. L.; Berthiaume, F. Elastin-like polypeptides: A strategic fusion partner for biologics. *Biotechnol. Bioeng.* **2016**, *113*, 1617–1627.
[133] Straley, K. S.; Heilshorn, S. C. Independent tuning of multiple biomaterial properties using protein engineering. *Soft Matter* **2009**, *5*, 114–124.
[134] Catherine, C.; Oh, S. J.; Lee, K. H.; Min, S. E.; Won, J. I.; Yun, H.; Kim, D. M. Engineering thermal properties of elastin-like polypeptides by incorporation of unnatural amino acids in a cell-free protein synthesis system. *Biotechnol. Bioprocess Eng.* **2015**, *20*, 417–422.
[135] Bataille, L.; Dieryck, W.; Hocquellet, A.; Cabanne, C.; Bathany, K.; Lecommandoux, S.; Garbay, B.; Garanger, E. Recombinant production and purification of short hydrophobic elastin-like polypeptides with low transition temperatures. *Protein Exp. Purif.* **2016**, *121*, 81–87.
[136] Urry, D. W.; Trapane, T. L.; Prasad, K. U. Phase-structure transitions of the elastin polypentapeptide–water system within the framework of composition–temperature studies. *Biopolymers* **1985**, *24*, 2345–2356.
[137] Urry, D. W. Physical chemistry of biological free energy transduction as demonstrated by elastic protein-based polymers. *J. Phys. Chem. B* **1997**, *101*, 11007–11028.
[138] Dhandhukia, J. P.; Shi, P.; Peddi, S.; Li, Z.; Aluri, S.; Ju, Y. P.; Brill, D.; Wang, W.; Janib, S. M.; Lin, Y. A. et al. Bifunctional elastin-like polypeptide nanoparticles bind rapamycin and integrins and suppress tumor growth *in vivo*. *Bioconjug. Chem.* **2017**, *28*, 2715–2728.
[139] Utterström, J.; Naeimipour, S.; Selegård, R.; Aili, D. Coiled coil-based therapeutics and drug delivery systems. *Adv. Drug Deliv. Rev.* **2021**, *170*, 26–43.
[140] Liu, J.; Zheng, Q.; Deng, Y. Q.; Cheng, C. S.; Kallenbach, N. R.; Lu, M. A seven-helix coiled coil. *Proc. Natl. Acad. Sci. USA* **2006**, *103*, 15457–15462.
[141] Lupas, A. N.; Bassler, J.; Dunin-Horkawicz, S. The structure and topology of α-helical coiled coils. In *Fibrous Proteins: Structures and Mechanisms*. Parry, D. A. D.; Squire, J. M. , Eds.; Springer: Cham, 2017; pp 95–129.
[142] Apostolovic, B.; Klok, H. A. pH-sensitivity of the E3/K3 heterodimeric coiled coil. *Biomacromolecules* **2008**, *9*, 3173–3180.
[143] Fletcher, J. M.; Harniman, R. L.; Barnes, F. R. H.; Boyle, A. L.; Collins, A.; Mantell, J.; Sharp, T. H.; Antognozzi, M.; Booth, P. J.; Linden, N. et al. Self-assembling cages from coiled-coil peptide modules. *Science* **2013**, *340*, 595–599.
[144] Ljubetič, A.; Lapenta, F.; Gradišar, H.; Drobnak, I.; Aupič, J.; Strmšek, Ž.; Lainšček, D.; Hafner-Bratkovič, I.; Majerle, A.; Krivec, N. et al. Design of coiled-coil protein-origami cages that self-assemble *in vitro* and *in vivo*. *Nat. Biotechnol.* **2017**, *35*, 1094–1101.
[145] Raman, S.; Machaidze, G.; Lustig, A.; Aebi, U.; Burkhard, P. Structure-based design of peptides that self-assemble into regular polyhedral nanoparticles. *Nanomed. Nanotechnol. Biol. Med.* **2006**, *2*, 95–102.
[146] Beck, K.; Gambee, J. E.; Kamawal, A.; Bächinger, H. P. A single amino acid can switch the oligomerization state of the α-helical coiled-coil domain of cartilage matrix protein. *EMBO J.* **1997**, *16*, 3767–3777.
[147] Dames, S. A.; Kammerer, R. A.; Wiltscheck, R.; Engel, J.; Alexandrescu, A. T. NMR structure of a parallel homotrimeric coiled coil. *Nat. Struct. Biol.* **1998**, *5*, 687–691.
[148] Klatt, A. R.; Becker, A. K. A.; Neacsu, C. D.; Paulsson, M.; Wagener, R. The matrilins: Modulators of extracellular matrix assembly. *Int. J. Biochem. Cell Biol.* **2011**, *43*, 320–330.
[149] Wiltscheck, R.; Dames, S. A.; Alexandrescu, A. T.; Kammerer, R. A.; Schulthess, T.; Blommers, M. J. J.; Engel, J. Heteronuclear NMR assignments and secondary structure of the coiled coil trimerization domain from cartilage matrix protein in oxidized and reduced forms. *Protein Sci.* **1997**, *6*, 1734–1745.
[150] Eriksson, M.; Hassan, S.; Larsson, R.; Linder, S.; Ramqvist, T.; Lövborg, H.; Vikinge, T.; Figgemeier, E.; Müller, J.; Stetefeld, J. et al. Utilization of a right-handed coiled-coil protein from archaebacterium staphylothermus marinus as a carrier for cisplatin. *Anticancer Res.* **2009**, *29*, 11–18.
[151] Fan, J. Q.; Fan, Y.; Wei, Z. J.; Li, Y. J.; Li, X. D.; Wang, L.; Wang, H. Transformable peptide nanoparticles inhibit the migration of N-cadherin overexpressed cancer cells. *Chin. Chem. Lett.* **2020**, *31*, 1787–1791.
[152] Zhou, X. Y.; Su, X. K.; Zhou, C. C. Preparation of diblock amphiphilic polypeptide nanoparticles for medical applications. *Eur. Polym. J.* **2018**, *100*, 132–136.
[153] Choi, H.; Liu, T.; Nath, K.; Zhou, R.; Chen, I. W. Peptide nanoparticle with pH-sensing cargo solubility enhances cancer drug efficiency. *Nano Today* **2017**, *13*, 15–22.
[154] Sigg, S. J.; Postupalenko, V.; Duskey, J. T.; Palivan, C. G.; Meier, W. Stimuli-responsive codelivery of oligonucleotides and drugs by self-assembled peptide nanoparticles. *Biomacromolecules* **2016**, *17*, 935–945.
[155] Gong, Z. Y.; Lao, J.; Gao, F.; Lin, W. P.; Yu, T.; Zhou, B. L.; Dong, J. H.; Liu, H.; Bai, J. K. pH-triggered geometrical shape switching of a cationic peptide nanoparticle for cellular uptake and drug delivery. *Colloids Surf. B Biointerfaces* **2020**, *188*, 110811.
[156] Gong, Z. Y.; Liu, X. Y.; Zhou, B. L.; Wang, G. H.; Guan, X. W.; Xu, Y.; Zhang, J. J.; Hong, Z. X.; Cao, J. J.; Sun, X. R. et al. Tumor acidic microenvironment-induced drug release of RGD peptide nanoparticles for cellular uptake and cancer therapy. *Colloids Surf. B Biointerfaces* **2021**, *202*, 111673.
[157] Cabral, H.; Matsumoto, Y.; Mizuno, K.; Chen, Q.; Murakami, M.; Kimura, M.; Terada, Y.; Kano, M. R.; Miyazono, K.; Uesaka, M. et al. Accumulation of sub-100 nm polymeric micelles in poorly permeable tumours depends on size. *Nat. Nanotechnol.* **2011**, *6*, 815–823.
[158] Raj, S.; Khurana, S.; Choudhari, R.; Kesari, K. K.; Kamal, M. A.; Garg, N.; Ruokolainen, J.; Das, B. C.; Kumar, D. Specific targeting cancer cells with nanoparticles and drug delivery in cancer therapy. *Semin. Cancer Biol.* **2021**, *69*, 166–177.
[159] Chithrani, B. D.; Ghazani, A. A.; Chan, W. C. W. Determining the size and shape dependence of gold nanoparticle uptake into mammalian cells. *Nano Lett.* **2006**, *6*, 662–668.
[160] Hoshyar, N.; Gray, S.; Han, H. B.; Bao, G. The effect of nanoparticle size on *in vivo* pharmacokinetics and cellular interaction. *Nanomedicine* **2016**, *11*, 673–692.
[161] Li, H. L.; Li, J. M.; He, X. Y.; Zhang, B.; Liu, C. X.; Li, Q. F.; Zhu, Y.; Huang, W. L.; Zhang, W.; Qian, H. et al. Histology and antitumor activity study of PTX-loaded micelle, a fluorescent drug delivery system prepared by PEG-TPP. *Chin. Chem. Lett.* **2019**, *30*, 1083–1088.
[162] Huang, K. Z.; Gao, M. Y.; Fan, L.; Lai, Y. Y.; Fan, H. W.; Hua, Z. Z. IR820 covalently linked with self-assembled polypeptide for photothermal therapy applications in cancer. *Biomater. Sci.* **2018**, *6*, 2925–2931.
[163] Huang, X.; Yin, Y. L.; Wu, M.; Zan, W.; Yang, Q. LyP-1 peptide-functionalized gold nanoprisms for SERRS imaging and tumor growth suppressing by PTT induced-hyperthermia. *Chin. Chem. Lett.* **2019**, *30*, 1335–1340.
[164] Wen, S. F.; Zhang, K.; Li, Y.; Fan, J. Q.; Chen, Z. M.; Zhang, J. P.; Wang, H.; Wang, L. A self-assembling peptide targeting VEGF receptors to inhibit angiogenesis. *Chin. Chem. Lett.* **2020**, *31*, 3153–3157.

[165] Peng, J. F.; Wang, R. R.; Sun, W. R.; Huang, M. H.; Wang, R.; Li, Y. J.; Wang, P. Y.; Sun, G. B.; Xie, S. Y. Delivery of miR-320a-3p by gold nanoparticles combined with photothermal therapy for directly targeting Sp1 in lung cancer. *Biomater. Sci.* **2021**, *9*, 6528–6541.

[166] Xiao, Y. J.; Zhang, Q.; Wang, Y. Y.; Wang, B.; Sun, F. N.; Han, Z. Y.; Feng, Y. Q.; Yang, H. T.; Meng, S. X.; Wang, Z. F. Dual-functional protein for one-step production of a soluble and targeted fluorescent dye. *Theranostics* **2018**, *8*, 3111–3125.

[167] Fan, R. R.; Mei, L.; Gao, X.; Wang, Y. L.; Xiang, M. L.; Zheng, Y.; Tong, A. P.; Zhang, X. N.; Han, B.; Zhou, L. X. et al. Self-assembled bifunctional peptide as effective drug delivery vector with powerful antitumor activity. *Adv. Sci.* **2017**, *4*, 1600285.

[168] Pastorino, F.; Brignole, C.; Marimpietri, D.; Cilli, M.; Gambini, C.; Ribatti, D.; Longhi, R.; Allen, T. M.; Corti, A.; Ponzoni, M. Vascular damage and anti-angiogenic effects of tumor vessel-targeted liposomal chemotherapy. *Cancer Res.* **2003**, *63*, 7400–7409.

[169] Garde, S. V.; Forté, A. J.; Ge, M.; Lepekhin, E. A.; Panchal, C. J.; Rabbani, S. A.; Wu, J. J. Binding and internalization of NGR-peptide-targeted liposomal doxorubicin (TVT-DOX) in CD13-expressing cells and its antitumor effects. *Anti-Cancer Drugs* **2007**, *18*, 1189–1200.

[170] Negussie, A. H.; Miller, J. L.; Reddy, G.; Drake, S. K.; Wood, B. J.; Dreher, M. R. Synthesis and *in vitro* evaluation of cyclic NGR peptide targeted thermally sensitive liposome. *J. Controlled Release* **2010**, *143*, 265–273.

[171] Sudimack, J.; Lee, R. J. Targeted drug delivery via the folate receptor. *Adv. Drug Deliv. Rev.* **2000**, *41*, 147–162.

[172] Lu, Y. J.; Low, P. S. Folate-mediated delivery of macromolecular anticancer therapeutic agents. *Adv. Drug Deliv. Rev.* **2012**, *64*, 342–352.

[173] Thong, Q. X.; Biabanikhankahdani, R.; Ho, K. L.; Alitheen, N. B.; Tan, W. S. Thermally-responsive virus-like particle for targeted delivery of cancer drug. *Sci. Rep.* **2019**, *9*, 3945.

[174] Chen, H. M.; Qin, Z. N.; Zhao, J. M.; He, Y.; Ren, E.; Zhu, Y.; Liu, G.; Mao, C. B.; Zheng, L. Cartilage-targeting and dual MMP-13/pH responsive theranostic nanoprobes for osteoarthritis imaging and precision therapy. *Biomaterials* **2019**, *225*, 119520.

[175] Högemann-Savellano, D.; Bos, E.; Blondet, C.; Sato, F.; Abe, T.; Josephson, L.; Weissleder, R.; Gaudet, J.; Sgroi, D.; Peters, P. J. et al. The transferrin receptor: A potential molecular imaging marker for human cancer. *Neoplasia* **2003**, *5*, 495–506.

[176] Mendes-Jorge, L.; Ramos, D.; Valença, A.; López-Luppo, M.; Pires, V. M. R.; Catita, J.; Nacher, V.; Navarro, M.; Carretero, A.; Rodriguez-Baeza, A. et al. L-ferritin binding to scara5: A new iron traffic pathway potentially implicated in retinopathy. *PLoS One* **2014**, *9*, e106974.

[177] Dong, Y. X.; Ma, Y. M.; Li, X.; Wang, F.; Zhang, Y. ERK-peptide-inhibitor-modified ferritin enhanced the therapeutic effects of paclitaxel in cancer cells and spheroids. *Mol. Pharm.* **2021**, *18*, 3365–3377.

[178] Owens III, D. E.; Peppas, N. A. Opsonization, biodistribution, and pharmacokinetics of polymeric nanoparticles. *Int. J. Pharm.* **2006**, *307*, 93–102.

[179] Singh, A.; Xu, J.; Mattheolabakis, G.; Amiji, M. EGFR-targeted gelatin nanoparticles for systemic administration of gemcitabine in an orthotopic pancreatic cancer model. *Nanomed. Nanotechnol. Biol. Med.* **2016**, *12*, 589–600.

[180] Hu, H.; Steinmetz, N. F. Doxorubicin-loaded physalis mottle virus particles function as a pH-responsive prodrug enabling cancer therapy. *Biotechnol. J.* **2020**, *15*, 2000077.

[181] Wang, C. Y.; Zhang, C.; Li, Z. L.; Yin, S.; Wang, Q.; Guo, F. X.; Zhang, Y.; Yu, R.; Liu, Y. D.; Su, Z. G. Extending half life of H-ferritin nanoparticle by fusing albumin binding domain for doxorubicin encapsulation. *Biomacromolecules* **2018**, *19*, 773–781.

[182] Jin, P. P.; Sha, R.; Zhang, Y. J.; Liu, L.; Bian, Y. P.; Qian, J.; Qian, J. Y.; Lin, J.; Ishimwe, N.; Hu, Y. et al. Blood circulation-prolonging peptides for engineered nanoparticles identified via phage display. *Nano Lett.* **2019**, *19*, 1467–1478.

[183] Chen, Y. X.; Wei, C. X.; Lyu, Y. Q.; Chen, H. Z.; Jiang, G.; Gao, X. L. Biomimetic drug-delivery systems for the management of brain diseases. *Biomater. Sci.* **2020**, *8*, 1073–1088.

[184] Zhang, H. Y.; Van Os, W. L.; Tian, X. B.; Zu, G. Y.; Ribovski, L.; Bron, R.; Bussmann, J.; Kros, A.; Liu, Y.; Zuhorn, I. S. Development of curcumin-loaded zein nanoparticles for transport across the blood-brain barrier and inhibition of glioblastoma cell growth. *Biomater. Sci.* **2021**, *9*, 7092–7103.

[185] Wen, L. J.; Peng, Y.; Wang, K.; Huang, Z. H.; He, S. Y.; Xiong, R. W.; Wu, L. P.; Zhang, F. T.; Hu, F. Q. Regulation of pathological BBB restoration via nanostructured ROS-responsive glycolipid-like copolymer entrapping siVEGF for glioblastoma targeted therapeutics. *Nano Res.* **2022**, *15*, 1455–1465.

[186] Li, Y. R.; Zhang, X. J.; Qi, Z. F.; Guo, X. L.; Liu, X. P.; Shi, W. J.; Liu, Y.; Du, L. B. The enhanced protective effects of salvianic acid A: A functionalized nanoparticles against ischemic stroke through increasing the permeability of the blood-brain barrier. *Nano Res.* **2020**, *13*, 2791–2802.

[187] Pang, H. H.; Huang, C. Y.; Chou, Y. W.; Lin, C. J.; Zhou, Z. L.; Shiue, Y. L.; Wei, K. C.; Yang, H. W. Bioengineering fluorescent virus-like particle/RNAi nanocomplexes act synergistically with temozolomide to eradicate brain tumors. *Nanoscale* **2019**, *11*, 8102–8109.

[188] Liu, W.; Lin, Q.; Fu, Y.; Huang, S. Q.; Guo, C. Q.; Li, L.; Wang, L. L.; Zhang, Z. R.; Zhang, L. Target delivering paclitaxel by ferritin heavy chain nanocages for glioma treatment. *J. Controlled Release* **2020**, *323*, 191–202.

[189] Huang, C. W.; Chuang, C. P.; Chen, Y. J.; Wang, H. Y.; Lin, J. J.; Huang, C. Y.; Wei, K. C.; Huang, F. T. Integrin $\alpha_2\beta_1$-targeting ferritin nanocarrier traverses the blood-brain barrier for effective glioma chemotherapy. *J. Nanobiotechnol.* **2021**, *19*, 180.

[190] Zhao, S.; Duan, H. X.; Yang, Y. L.; Yan, X. Y.; Fan, K. L. Fenozyme protects the integrity of the blood-brain barrier against experimental cerebral malaria. *Nano Lett.* **2019**, *19*, 8887–8895.

[191] Chen, Z. Y.; Liao, T.; Wan, L. H.; Kuang, Y.; Liu, C.; Duan, J. L.; Xu, X. Y.; Xu, Z. Q.; Jiang, B. B.; Li, C. Dual-stimuli responsive near-infrared emissive carbon dots/hollow mesoporous silica-based integrated theranostics platform for real-time visualized drug delivery. *Nano Res.* **2021**, *14*, 4264–4273.

[192] Li, H. P.; Zhou, Z. W.; Zhang, F. R.; Guo, Y. X.; Yang, X.; Jiang, H. L.; Tan, F.; Oupicky, D.; Sun, M. J. A networked swellable dextrin nanogels loading Bcl2 siRNA for melanoma tumor therapy. *Nano Res.* **2018**, *11*, 4627–4642.

[193] Yao, H. C.; Zhao, W. W.; Zhang, S. G.; Guo, X. F.; Li, Y.; Du, B. Dual-functional carbon dot-labeled heavy-chain ferritin for self-targeting bio-imaging and chemo-photodynamic therapy. *J. Mater. Chem. B* **2018**, *6*, 3107–3115.

[194] Niikura, K.; Sugimura, N.; Musashi, Y.; Mikuni, S.; Matsuo, Y.; Kobayashi, S.; Nagakawa, K.; Takahara, S.; Takeuchi, C.; Sawa, H. et al. Virus-like particles with removable cyclodextrins enable glutathione-triggered drug release in cells. *Mol. BioSyst.* **2013**, *9*, 501–507.

[195] Aljabali, A. A. A.; Shukla, S.; Lomonossoff, G. P.; Steinmetz, N. F.; Evans, D. J. CPMV-DOX delivers. *Mol. Pharm.* **2013**, *10*, 3–10.

[196] Nguyen, B.; Tolia, N. H. Protein-based antigen presentation platforms for nanoparticle vaccines. *npj Vaccines* **2021**, *6*, 70.

[197] Gobeil, P.; Pillet, S.; Boulay, I.; Séguin, A.; Makarkov, A.; Heizer, G.; Bhutada, K.; Mahmood, A.; Charland, N.; Trépanier, S. et al. Phase 2 randomized trial of an AS03 adjuvanted plant-based virus-like particle vaccine for Covid-19 in healthy adults, older adults and adults with comorbidities. *medRxiv*, in press, https://doi.org/10.1101/2021.05.14.21257248.

[198] Ward, B. J.; Séguin, A.; Couillard, J.; Trépanier, S.; Landry, N. Phase III: Randomized observer-blind trial to evaluate lot-to-lot consistency of a new plant-derived quadrivalent virus like particle influenza vaccine in adults 18–49 years of age. *Vaccine* **2021**, *39*, 1528–1533.

[199] Chichester, J. A.; Green, B. J.; Jones, R. M.; Shoji, Y.; Miura, K.; Long, C. A.; Lee, C. K.; Ockenhouse, C. F.; Morin, M. J.; Streatfield, S. J. et al. Safety and immunogenicity of a plant-

produced Pfs25 virus-like particle as a transmission blocking vaccine against malaria: A phase 1 dose-escalation study in healthy adults. *Vaccine* **2018**, *36*, 5865–5871.

[200] Pillet, S.; Aubin, É.; Trépanier, S.; Poulin, J. F.; Yassine-Diab, B.; Meulen, J. T.; Ward, B. J.; Landry, N. Humoral and cell-mediated immune responses to H5N1 plant-made virus-like particle vaccine are differentially impacted by alum and GLA-SE adjuvants in a phase 2 clinical trial. *npj Vaccines* **2018**, *3*, 3.

[201] Chichester, J. A.; Jones, R. M.; Green, B. J.; Stow, M.; Miao, F. D.; Moonsammy, G.; Streatfield, S. J.; Yusibov, V. Safety and immunogenicity of a plant-produced recombinant hemagglutinin-based influenza vaccine (HAI-05) derived from A/indonesia/05/2005 (H5N1) influenza virus: A phase 1 randomized, double-blind, placebo-controlled, dose-escalation study in healthy adults. *Viruses* **2012**, *4*, 3227–3244.

[202] Cummings, J. F.; Guerrero, M. L.; Moon, J. E.; Waterman, P.; Nielsen, R. K.; Jefferson, S.; Gross, F. L.; Hancock, K.; Katz, J. M.; Yusibov, V. Safety and immunogenicity of a plant-produced recombinant monomer hemagglutinin-based influenza vaccine derived from influenza a (H1N1)pdm09 virus: A phase 1 dose-escalation study in healthy adults. *Vaccine* **2014**, *32*, 2251–2259.

[203] Ortega-Rivera, O. A.; Shin, M. D.; Chen, A.; Beiss, V.; Moreno-Gonzalez, M. A.; Lopez-Ramirez, M. A.; Reynoso, M.; Wang, H.; Hurst, B. L.; Wang, J. et al. Trivalent subunit vaccine candidates for COVID-19 and their delivery devices. *J. Am. Chem. Soc.* **2021**, *143*, 14748–14765.

[204] Christiansen, D.; Earnest-Silveira, L.; Chua, B.; Meuleman, P.; Boo, I.; Grubor-Bauk, B.; Jackson, D. C.; Keck, Z. Y.; Foung, S. K. H.; Drummer, H. E. et al. Immunological responses following administration of a genotype 1a/1b/2/3a quadrivalent HCV VLP vaccine. *Sci. Rep.* **2018**, *8*, 6483.

[205] Zabel, F.; Mohanan, D.; Bessa, J.; Link, A.; Fettelschoss, A.; Saudan, P.; Kündig, T. M.; Bachmann, M. F. Viral particles drive rapid differentiation of memory B cells into secondary plasma cells producing increased levels of antibodies. *J. Immunol.* **2014**, *192*, 5499–5508.

[206] Gomes, A. C.; Mohsen, M.; Bachmann, M. F. Harnessing nanoparticles for immunomodulation and vaccines. *Vaccines* **2017**, *5*, 6.

[207] Kanekiyo, M.; Wei, C. J.; Yassine, H. M.; McTamney, P. M.; Boyington, J. C.; Whittle, J. R. R.; Rao, S. S.; Kong, W. P.; Wang, L. S.; Nabel, G. J. Self-assembling influenza nanoparticle vaccines elicit broadly neutralizing H1N1 antibodies. *Nature* **2013**, *499*, 102–106.

[208] Kang, Y. F.; Sun, C.; Zhuang, Z.; Yuan, R. Y.; Zheng, Q. B.; Li, J. P.; Zhou, P. P.; Chen, X. C.; Liu, Z.; Zhang, X. et al. Rapid development of SARS-CoV-2 spike protein receptor-binding domain self-assembled nanoparticle vaccine candidates. *ACS Nano* **2021**, *15*, 2738–2752.

[209] Bruun, T. U. J.; Andersson, A. M. C.; Draper, S. J.; Howarth, M. Engineering a rugged nanoscaffold to enhance plug-and-display vaccination. *ACS Nano* **2018**, *12*, 8855–8866.

[210] Hsia, Y.; Bale, J. B.; Gonen, S.; Shi, D.; Sheffler, W.; Fong, K. K.; Nattermann, U.; Xu, C.; Huang, P.-S.; Ravichandran, R. et al. Corrigendum: Design of a hyperstable 60-subunit protein icosahedron. *Nature* **2016**, *540*, 150.

[211] Bale, J. B.; Gonen, S.; Liu, Y. X.; Sheffler, W.; Ellis, D.; Thomas, C.; Cascio, D.; Yeates, T. O.; Gonen, T.; King, N. P. et al. Accurate design of megadalton-scale two-component icosahedral protein complexes. *Science* **2016**, *353*, 389–394.

[212] Babapoor, S.; Neef, T.; Mittelholzer, C.; Girshick, T.; Garmendia, A.; Shang, H. W.; Khan, M. I.; Burkhard, P. A novel vaccine using nanoparticle platform to present immunogenic M2e against avian influenza infection. *Influenza Res. Treat.* **2011**, *2011*, 126794.

[213] Champion, C. I.; Kickhoefer, V. A.; Liu, G. C.; Moniz, R. J.; Freed, A. S.; Bergmann, L. L.; Vaccari, D.; Raval-Fernandes, S.; Chan, A. M.; Rome, L. H. et al. A vault nanoparticle vaccine induces protective mucosal immunity. *PLoS One* **2009**, *4*, e5409.

[214] Hu, H.; Steinmetz, N. F. Development of a virus-like particle-based anti-HER2 breast cancer vaccine. *Cancers* **2021**, *13*, 2909.

[215] Wang, W. J.; Liu, Z. D.; Zhou, X. X.; Guo, Z. Q.; Zhang, J.; Zhu, P.; Yao, S.; Zhu, M. Z. Ferritin nanoparticle-based SpyTag/SpyCatcher-enabled click vaccine for tumor immunotherapy. *Nanomed. Nanotechnol. Biol. Med.* **2019**, *16*, 69–78.

[216] Rad-Malekshahi, M.; Fransen, M. F.; Krawczyk, M.; Mansourian, M.; Bourajjaj, M.; Chen, J.; Ossendorp, F.; Hennink, W. E.; Mastrobattista, E.; Amidi, M. Self-assembling peptide epitopes as novel platform for anticancer vaccination. *Mol. Pharm.* **2017**, *14*, 1482–1493.